Journal of Vacuum Science and Technology A

RESEARCH ARTICLE | SEPTEMBER 24 2020

Introduction to x-ray photoelectron spectroscopy

Special Collection: Special Topic Collection: Reproducibility Challenges and Solutions

Fred A. Stevie; Carrie L. Donley

J. Vac. Sci. Technol. A 38, 063204 (2020)
https://doi.org/10.1116/6.0000412

JVST A
Journal of Vacuum Science & Technology A

ARTICLE

avs.scitation.org/journal/jva

Introduction to x-ray photoelectron spectroscopy

Cite as: J. Vac. Sci. Technol. A 38, 063204 (2020); doi: 10.1116/6.0000412
Submitted: 22 June 2020 · Accepted: 31 August 2020 ·
Published Online: 24 September 2020

Fred A. Stevie[1,a)] and Carrie L. Donley[2,b)]

AFFILIATIONS

[1]Analytical Instrumentation Facility, North Carolina State University, Raleigh, North Carolina 27695
[2]Chapel Hill Analytical and Nanofabrication Laboratory, University of North Carolina, Chapel Hill, North Carolina 27599

Note: This paper is part of the Special Topic Collection on Reproducibility Challenges and Solutions.
[a)]**Electronic mail:** fred_stevie@ncsu.edu
[b)]**Electronic mail:** cdonley@email.unc.edu

ABSTRACT

X-ray photoelectron spectroscopy (XPS) has become one of the most widely used surface analysis techniques, and XPS instrumentation has become more user friendly, making the technique available to a large number of researchers. The number of experts in the field, however, has not increased, and XPS data are often misinterpreted in the literature. This paper is intended to provide an introduction to XPS for prospective or novice users. We present the basic principles of the technique including (1) the photoelectric effect, (2) how electrons interact with matter and escape from a surface and how this determines the surface sensitivity of the technique, and (3) how the chemical environment around an element affects the binding energy of its electrons. A description of the instrumentation helps a novice user understand how data are acquired, and information is included on sample preparation and mounting. The important parameters for data acquisition are noted to help guide users starting to acquire data. Interpretation of data on both a qualitative and quantitative level is discussed, and additional sections provide information on more advanced techniques such as angle resolved XPS, small area analysis, near ambient pressure XPS, valence XPS, and ultraviolet photoelectron spectroscopy.

I. INTRODUCTION

This article is part of a collection of guides and tutorials[1] intended to provide a basic understanding of important topics involving the application of x-ray photoelectron spectroscopy (XPS), one of the most widely used surface sensitive techniques available. Recent articles have documented the common misinterpretation of materials science characterization data in the literature.[2,3] Materials analysis techniques such as XPS have become more widely available and user friendly, while the number of true experts for these techniques has not increased. As a result, many novice users of a technique such as XPS attempt to interpret data on their own and often get it wrong. The goal of this paper is to summarize the experience of the authors, who frequently work with potential and novice users, and information found in many books and other publications,[4–11] in order to provide an appropriate introduction to XPS. While this paper is intended as a first step for novice XPS users to learn more about the technique, they are encouraged to consult with those with more experience. XPS systems are often located in shared user facilities, and those facility staff are great resources to advise researchers with regard to the collection and interpretation of XPS data.

This paper introduces important concepts needed to understand and apply XPS to a wide range of scientific and technological research topics and may help researchers to recognize and avoid some of the misinterpretation that appears in the literature. Periodically, issues or topics are identified in Caution Boxes that are beyond the scope of this paper but have been sources of confusion or errors in the literature. Other papers in this series provide additional information on topics introduced in this paper including quantification,[12,13] electron path lengths,[14] background signals and peak fitting,[15,16] instrument calibration,[17] and consistent terminology.[18]

X-ray photoelectron spectroscopy is a surface sensitive analytical technique, in which x-rays bombard the surface of a material and the kinetic energy of the emitted electrons is measured. The two major characteristics of this technique that make it powerful as an analytical method are its surface sensitivity and its ability to reveal chemical state information from the elements in the sample. All elements except hydrogen and helium can be detected, and XPS

has been used to study the surface of almost every material from plastics to textiles to soil to semiconductors. All materials have surfaces, and it is those surfaces that interact with other materials. Factors such as surface wettability, adhesion, corrosion, charge transfer, and catalysis are all determined by surfaces and surface contamination, and, therefore, studying and understanding surfaces is important.

XPS is based on the photoelectric effect, first discovered by Heinrich Hertz in 1887. He noticed that electrons were emitted from surfaces when irradiated with light. Albert Einstein more formally described the concept in 1905 and was awarded the Nobel Prize in physics in 1921 for this work. Photoemission from x-ray irradiation was first observed by Robinson and Rawlinson in 1914, and the first application of photoemission as an analysis method was presented by Steinhardt and Serfass in 1951.[19] However, the bulk of the work to develop x-ray photoelectron spectroscopy into the technique we know today was done by Kai Siegbahn at the University of Uppsala in Sweden in the 1950s and 1960s.[20–22] He won the Nobel Prize in 1981 for his work on high resolution electron spectroscopy, which was initially referred to as electron spectroscopy for chemical analysis (ESCA).

II. PRINCIPLES OF THE TECHNIQUE

A. Generation of photoelectrons

In XPS, the sample is irradiated with soft x-rays (energies lower than ~6 keV) and the kinetic energy of the emitted electrons is analyzed [Fig. 1(a)]. The emitted photoelectron is the result of complete transfer of the x-ray energy to a core level electron. This is expressed mathematically in Eq. (1). It simply states that the energy of the x-ray ($h\nu$) is equal to the binding energy (BE) of the electron (how tightly it is bound to the atom/orbital to which it is attached), plus the kinetic energy (KE) of the electron that is emitted, plus the spectrometer work function (Φ_{spec}), a constant value,

$$h\nu = BE + KE + \Phi_{spec}. \quad (1)$$

To determine the binding energy of an electron, Eq. (1) can be rearranged to obtain Eq. (2), where the terms on the right are either known ($h\nu$ and Φ_{spec}) or measured in the XPS experiment (KE),

$$BE = h\nu - KE - \Phi_{spec}. \quad (2)$$

This concept is also demonstrated diagrammatically in Fig. 2. Note that the photoelectron binding energy is measured with respect to the sample Fermi level (not the vacuum level) which is the reason that Φ_{spec} is included.

Photoelectron peaks are notated by the element and orbital from which they were ejected. For example, "O 1s" describes electrons emitted from the 1s orbital of an oxygen atom. Any electron with a binding energy less than the x-ray source energy should be emitted from the sample and observed with the XPS technique. The binding energy of an electron is a material property and is independent of the x-ray source used to eject it. When experiments are performed with different x-ray sources, the binding energy of photoelectrons will not change; however, the kinetic energy of the photoelectrons emitted will vary as described by Eq. (2).

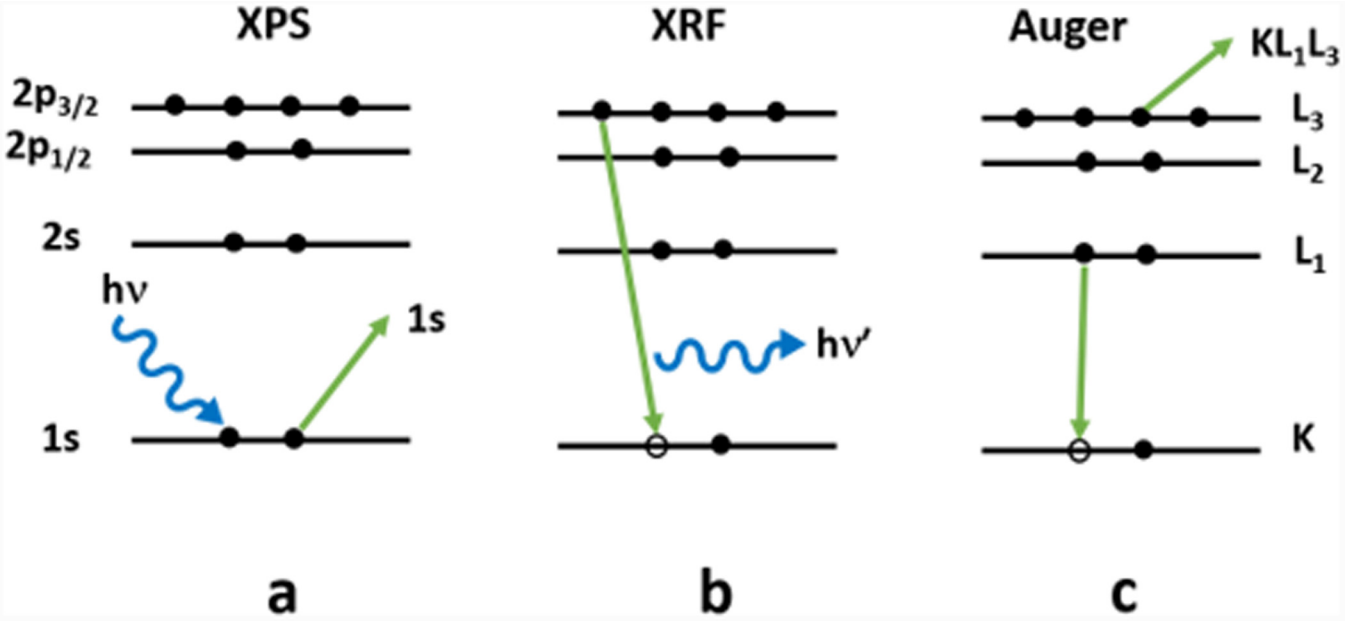

FIG. 1. Processes that result from x-ray bombardment of a surface include (a) emission of a photoelectron, (b) x-ray fluorescence, and (c) emission of an Auger electron.

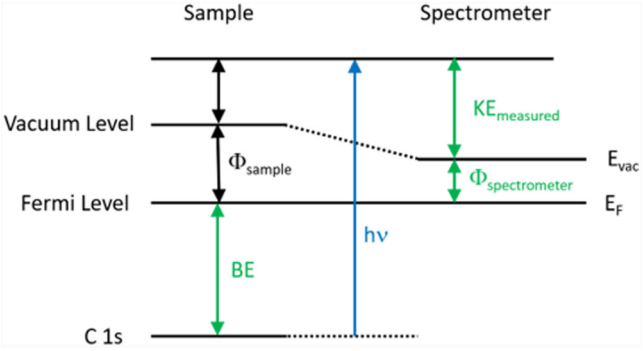

FIG. 2. Energy level diagram illustrates schematically the basic XPS equation, including the x-ray source energy (hυ), the binding energy of the electron (BE), the measured kinetic energy of the electron ($KE_{measured}$), and the work function of the spectrometer ($\Phi_{spectrometer}$).

B. Auger electrons

The loss of the XPS core electron results in a core "hole." This excited ionized state will relax by filling the hole with an electron from a valence orbital. This relaxation process releases energy in one of the two competing processes: x-ray fluorescence or the emission of an Auger electron. X-ray fluorescence [Fig. 1(b)] is not detected in the electron spectrum and will not be considered further here. Auger electrons generated by the process described in Fig. 1(c) will be detected and are often used in XPS for qualitative analysis.

The notation of Auger peaks traditionally relies on the K, L, and M nomenclature for atomic orbitals. For example, the main oxygen Auger peak is denoted by KLL, which indicates that the first ejected electron came from a K orbital, the electron that filled the core hole came from an L orbital, and the final Auger electron ejected also came from an L orbital. Subscripts are sometimes used to differentiate between specific L, M, and N orbitals as demonstrated in Fig. 1(c). The Auger process involves three different electron transitions, and the kinetic energy of the ejected Auger electron is described in Eq. (3) using a KLL transition as an example,

$$KE_{Auger} \sim BE(K) - BE(L_1) - BE(L_3). \quad (3)$$

The kinetic energy of the Auger electron depends on the binding energies of specific orbitals in the atom from which it

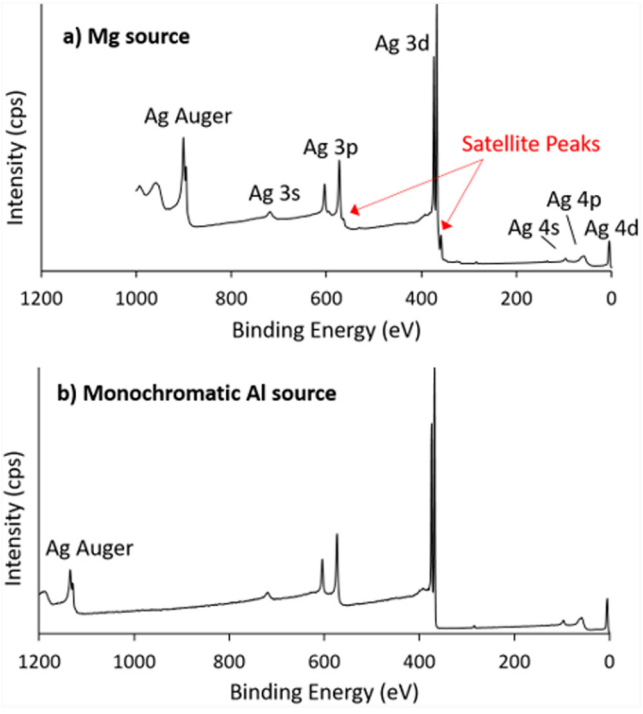

FIG. 3. Survey spectra for silver with (a) nonmonochromatic Mg and (b) monochromatic Al sources show how the photoelectron peaks are at the same binding energies but the Auger peaks shift with the use of different sources. Note that the satellite peaks are removed by the monochromator source as discussed in Sec. III.

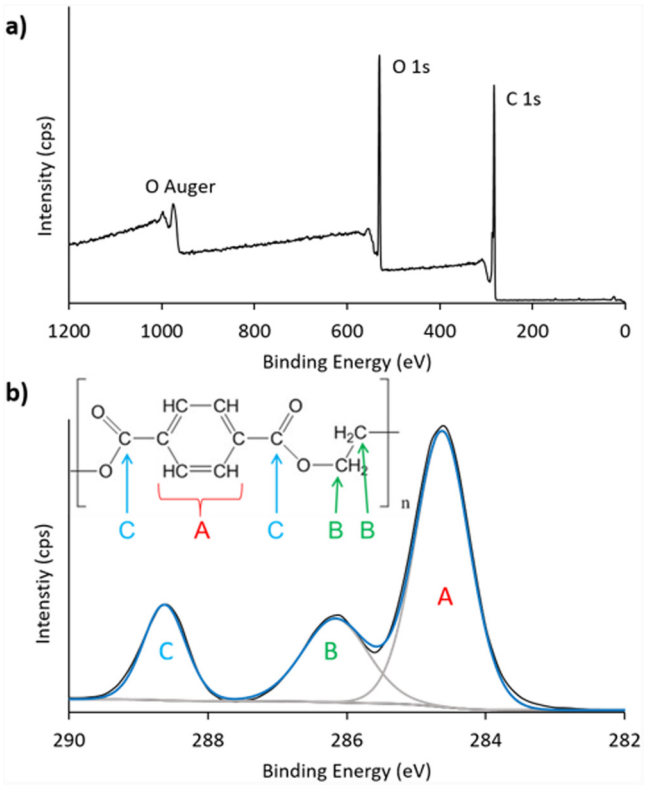

FIG. 4. XPS survey spectrum (a) and high-resolution C 1s spectrum (b) of PET. The inset of (b) shows the chemical structure of PET and the assignments of the three peaks in the C 1s spectrum.

originated. Since these binding energies are independent of the x-ray source energy, it follows that the kinetic energy of the Auger electron is also independent of the x-ray excitation energy. Thus, when different x-ray sources are used for excitation, the calculated binding energy of the Auger electrons will change. The fact that the binding energy of photoelectrons is constant with the x-ray source, while the binding energy of Auger electrons changes, is useful when spectral overlaps between Auger lines and photoelectron lines occur. Using a different x-ray source can often separate those overlaps as demonstrated in Fig. 3. The most intense silver Auger peak is observed at a binding energy of 902 eV with Mg x-ray excitation, but at 1135 eV when an Al x-ray source is used.

C. Chemical environment

XPS survey and high-resolution C 1s spectra of polyethylene terephthalate (PET) are shown in Fig. 4. Note that the y axis is typically intensity in counts/s and the x axis is the binding energy in electron volts, with the convention of binding energy decreasing from left to right. Survey spectra are typically used to obtain basic elemental information and to look for the presence of unexpected elements in the sample. Figure 4(a) shows that the PET sample contains carbon and oxygen as expected.

An important advantage of XPS over other techniques is the ability to determine the chemical environment of the atoms present in a sample. This chemical environment, including factors like nearest neighbors and the oxidation state of the element, affects the binding energy of the photoelectron peaks (and the Auger peaks). Let us examine this concept in more detail with the high-resolution C 1s peak from PET in Fig. 4(b). In the case of C 1s, the binding energy is highly dependent on the electronegativity of the nearest neighbor elements. As the neighboring atom becomes more electronegative, the binding energy for the C 1s electron increases as shown in Table I. XPS can easily distinguish between C—C, C—O, C═O, and C–F_2 based on this simple electronegativity trend. Therefore, peak assignments for the three C 1s peaks can be made as shown in Fig. 4(b). The relative area under each peak is representative of the number of carbon atoms present in each environment.

For most transition metals, the binding energy is primarily affected by the oxidation state of the metal. If an atom has already lost some electron density and exhibits a positive charge, it will be more difficult to remove an electron from that atom, and the binding energy will be higher. Table II shows binding energies for several titanium oxidation states, illustrating this trend of increasing binding energy as the oxidation state increases. Values of binding energies can be found in many texts and online sources.[24–38]

TABLE I. Binding energies for several carbon chemical states (Ref. 23), reprinted with permission from Ratner and Castner, in *Surface Analysis: The Principal Techniques*, edited by J. C. Vickerman (Wiley, Chichester, 2009). Copyright 2009, John Wiley & Sons.

Chemical state	Binding energy (eV)
C—C or C═C	285.0
C—N	286.0
C—O	286.5
C═O	288.0
O—C═O	289.0
CF_2	292.0
CF_3	293–294

TABLE II. Binding energies for several titanium chemical states for the Ti $2p_{3/2}$ orbital, (Ref. 35) reprinted with permission from NIST X-ray Photoelectron Spectroscopy Database, NIST Standard Reference Database Number 20, National Institute of Standards and Technology, Gaithersburg MD, 20899 (2012), doi:10.18434/T4T88K, see https://srdata.nist.gov/xps/main_search_menu.aspx. Copyright 2012, United States of America as represented by the Secretary of Commerce.

Chemical state	Oxidation state	Binding energy (eV)
Ti	Ti(0)	453.9
TiO	Ti(II)	455.2
TiO_2	Ti(IV)	458.7

Caution Box 1:

While the oxidation state of a material is a general guide to determining binding energy, it is not always the only factor that determines the peak position and peak shape. Binding energies determined for photoelectron peaks, as in Fig. 4(b) using Eq. (2) are not simply binding energies determined by the electron energy levels of the atom in the solid. Although the binding energies reported in Table II shift to higher energies with increasing oxidation, Ti in the same oxidation state can have significantly different peak shapes.[18] It would be more appropriate to identify the measured peak energies determined by XPS as measured BEs (BE_{meas}) to differentiate them from the actual binding energies determined from the atomic energy levels.

The measured binding energy involves transfer of an electron from an atom in an initial state leaving the atom in an excited final state. Although there is only one initial state, there may be many accessible final states, which can influence peak shape and measured energies. When there is only one final state, the initial state determines the measured binding energy, and the rules discussed in this section about neighboring atom electronegativity and oxidation state apply. But, in some cases, multiple final state effects are possible, and they can dominate the resulting spectra, causing multiplet splitting, shakeup, and shakeoff processes[18] (introduced in Sec. VI of this paper). These processes can cause broadened peaks or multiple peaks, and interpretation is more difficult, as the measured peak energies are not always simply related to the BE of the atomic states in the solid. It is important to check other results in the literature before assigning unexpected peaks as new or different chemical states.

D. Surface sensitivity

To understand why XPS is a surface sensitive technique, the physical processes that affect electrons traveling in solids must be examined. The x-rays that irradiate the sample can penetrate quite deeply (a few μm) into the sample. Electrons generated this deep in the sample will encounter many inelastic collisions (collisions that involve the loss of energy) and eventually will lose all their energy before escaping from the sample. In Fig. 5(a), the electrons labeled "C" represent these deeply generated electrons. Electrons generated nearer to the surface may have only one or two inelastic collisions before escaping from the sample and reaching the detector. These electrons leave the sample with less kinetic energy than expected, because they have lost some random amount of energy on their way to the detector. These electrons are labeled as "B" in Fig. 5(a); they contribute to the vertical step in the background signal that accompanies any large photoelectron or Auger electron peak as shown in Fig. 5(b). The background contribution from C 1s peaks is shaded in orange, and similar background contributions are made by the O 1s and O Auger peaks. Only the electrons that escape the surface without any inelastic collisions will contribute to the characteristic photoelectron peaks that we use in XPS analysis. These are labeled "A" in Figs. 5(a) and 5(b).

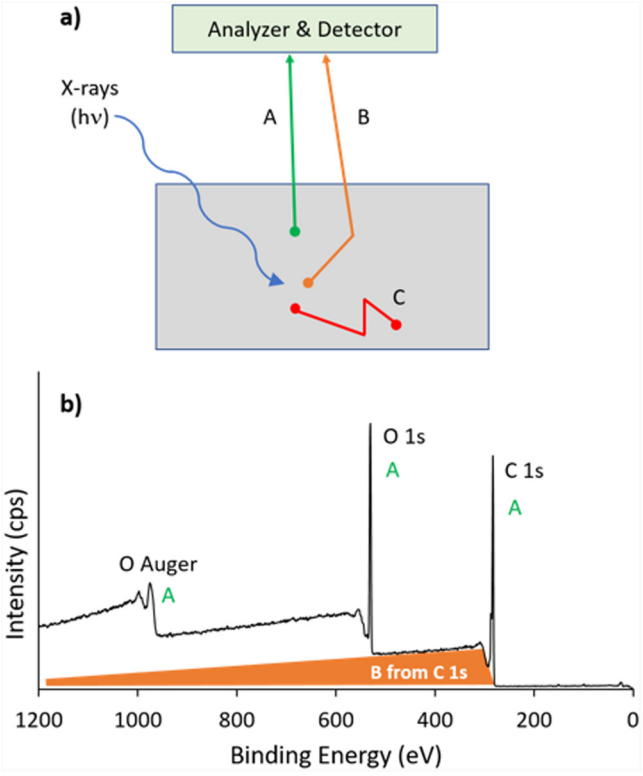

FIG. 5. Emitted electrons interact with the sample in different ways depending on the depth at which they are generated. In (a), electrons emitted without interaction, labeled A, produce XPS photoelectron and Auger peaks. Electrons which undergo at least one inelastic collision, labeled B, contribute to the background. Electrons that undergo multiple collisions and do not escape the sample are labeled C. (b) shows the XPS spectrum for PET with photoelectron and Auger peaks labeled. The orange shaded area shows the contribution to the background signal that results from C 1s electrons. While only the contribution to the background from C 1s electrons is illustrated here, similar background contributions are made by electrons from O 1s and O Auger transitions as well, forming the vertical "steps" in the baseline observed for every major peak.

The surface sensitivity of XPS is determined by how deep an electron can be generated and still escape without inelastically scattering. Beer's law describes the intensity, I, of electrons emitted from a sample at depths deeper than d, where I_0 represents the total number of electrons generated from the sample,

$$I = I_0 \exp(-d/\lambda). \quad (4)$$

The term λ is the attenuation length of the electron, which will depend on the energy of the electron and the material through which it is traveling. The attenuation length is similar to the inelastic mean free path (IMFP) of the electrons (defined as the average distance an electron with a certain kinetic energy can travel before inelastically scattering), but the attenuation length also takes into account the effect of elastic scattering. Detailed studies of both attenuation length and IMFP are beyond the scope of this text, but the interested reader can consult many references.[14,39–47] A plot of the universal curve of the inelastic mean free path as a function of electron kinetic energy is shown in Fig. 6.[41] Electrons with kinetic energies of ~1000 eV have an IMFP on the order of a few nm. Using Beer's law, it can be shown that about 95% of the electrons will escape from a depth of 10 nm or less, and 10 nm is often cited as the information depth for XPS. The information depth (commonly called the sampling depth) is defined as the maximum depth normal to the surface from which useful information is obtained,[14] and in this case, we define useful information as 95% of the total signal.

As Fig. 6 shows, for electrons typically analyzed with XPS (KE >100 eV), the IMFP increases as the kinetic energy of the electron increases. Higher energy X-ray sources generate electrons with higher kinetic energies [Eq. (2)], and, therefore, electrons will be able to escape from deeper within the sample. Common x-ray source energies are listed in Table III. Analysis with different x-ray sources allows the researcher to probe different depths within the

Caution Box 2:

In the early days of XPS, the information depth was thought to be completely controlled by inelastic scattering, and the IMFP was thought to be the controlling parameter. As the impact of elastic scattering was better understood, additional concepts evolved including attenuation length, mean escape depth, and information depth. IMFP is a true material parameter, while other lengths depend on specific measurement conditions and they can have a significant impact on careful quantitative measurements.[14,18]

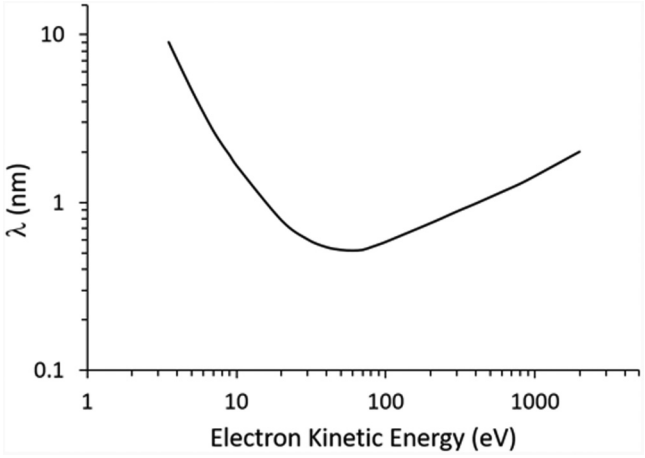

FIG. 6. Inelastic mean free path (IMFP or λ) is shown as a function of electron kinetic energy. Curve shape obtained from data found in Ref. 41.

sample. While the information depth for Si 2p electrons is ~7 nm for an aluminum source, it is closer to 22 nm for a chromium source.[48]

III. INSTRUMENTATION

An XPS instrument contains an x-ray source, sample stage, extraction lenses, analyzer, and detector housed in an ultra-high vacuum environment. A schematic diagram of an XPS system is shown in Fig. 7, illustrating all the main components that are discussed below. Detailed descriptions of instrument components can be found in Refs. 49–53.

XPS instruments are housed within ultra-high vacuum (UHV) environments for two reasons. First, the emitted electrons must not scatter off air molecules while traveling to the analyzer, and this requires vacuum levels on the order of 10^{-5}–10^{-6} mbar. In practice, XPS systems typically have much lower base pressures that are closer to 10^{-9}–10^{-10} mbar. Because XPS is a surface sensitive technique, it is very sensitive to surface contamination. At a pressure of 1×10^{-6} mbar and a sticking coefficient of 1 (every molecule that strikes the surface sticks to that surface), there would be one monolayer of contamination in 2 s! As a result, XPS instruments utilize the UHV environment to reduce the surface contamination that occurs within the chamber.

TABLE III. Commercially available x-ray sources.

Anode material	Energy (eV)	Natural linewidth (eV)
Mg	1253.6	0.7
Al	1486.6	0.9
Ag	2984.4	2.6
Cr	5417.0	2.1
Ga	9251.7	2.6

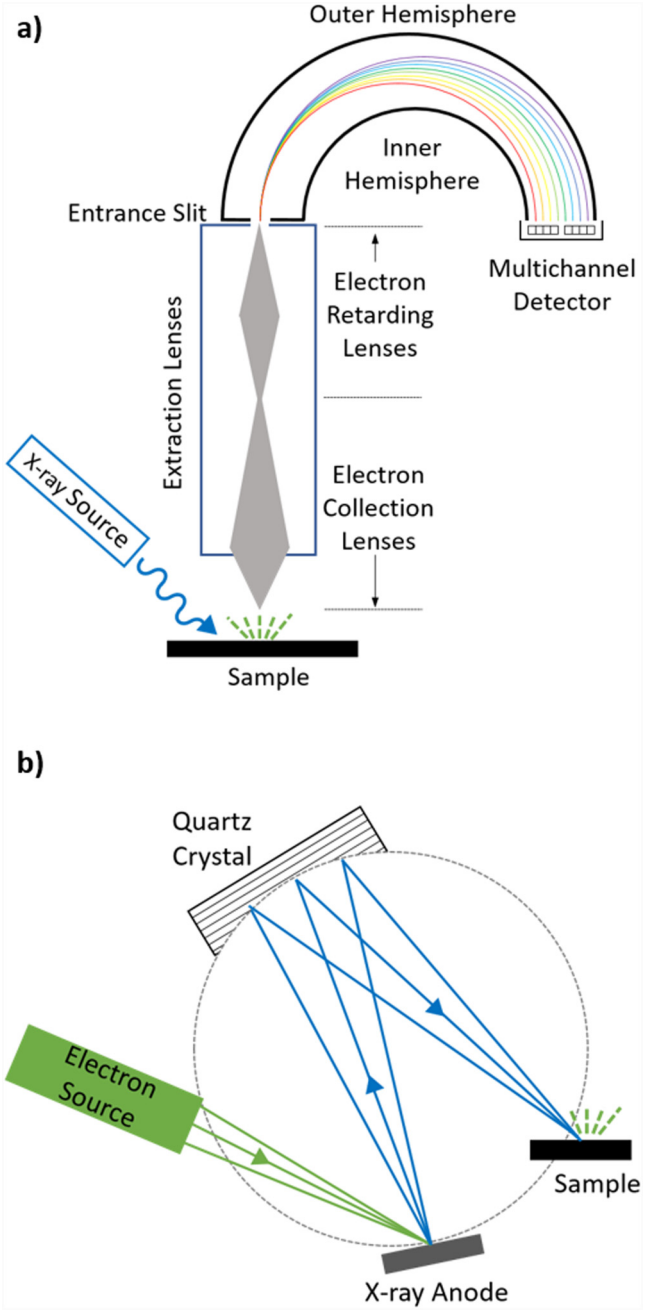

FIG. 7. Schematic diagrams show the major components of an (a) XPS instrument and (b) monochromator.

A. X-ray sources

X-ray sources use a heated tungsten or LaB_6 (lanthanum hexaboride) filament to provide a source of electrons that are accelerated toward a high voltage anode. The choice of the anode material depends on several factors:

(1) Energy: The energy of the source will determine the transitions that can be measured.
(2) Linewidth: For non-monochromatic sources, the natural linewidth will limit the resolution of the measurement. (Monochromatic sources offer much narrower linewidths.)
(3) Analysis depth: Higher energy sources will probe deeper in the sample.
(4) Ionization cross section: This measure of the probability that an atom will lose an electron due to x-ray irradiation decreases for higher kinetic energy electrons produced by higher energy sources.[54]

XPS systems were originally equipped with Al and/or Mg sources, often in the form of a dual anode source that contains both Al and Mg anodes which can be individually selected. Many instruments incorporate a monochromator, typically for an aluminum source. As shown in Fig. 7(b), aluminum x-ray monochromators utilize a quartz crystal positioned at a specific angle to allow only Al Kα x-rays to diffract, filtering out other Al x-ray lines and Bremsstrahlung radiation (continuous energy x-ray radiation produced by x-ray sources).[55,56] Repositioning the quartz crystal can also allow monochromatization of Ag Lα x-rays, and dual anode monochromatic Al/Ag sources are now available. Other monochromatic sources, such as chromium, can also be obtained.

There are several advantages to monochromatic sources and some manufacturers are moving toward instruments exclusively equipped with monochromatic sources. The first advantage is that the monochromator eliminates any excitation by x-ray lines other than the most intense main line. For example, a nonmonochromatic Mg x-ray source will irradiate the samples with the most intense Mg $K\alpha_{1,2}$ line but also with other less intense lines. The most intense of these other lines is the Mg $K\alpha_3$ with an energy that is 8.4 eV lower than the Mg $K\alpha_{1,2}$ line and an intensity that is 9.2% of the main line.[56] As a result, additional peaks due to excitation with multiple x-ray energies will appear in the XPS spectrum, and they are called satellite peaks. Figure 3 shows survey spectra of silver taken with a nonmonochromatic Mg source and a monochromatic Al source. The satellite peaks present with the Mg source are clearly absent when data are acquired with the monochromatic Al source. Similar satellite peaks are observed when a nonmonochromatic Al source is used.

XPS spectral resolution is limited by the x-ray linewidth. An additional advantage of a monochromatic source is reduced x-ray linewidth. For an aluminum source, the source linewidth decreases from 0.9 eV to approximately 0.25 eV when a monochromator is used.[57] The effect of using a source with a smaller linewidth is demonstrated in the high resolution Ag 3d peaks in Fig. 8, which show a much smaller full width half maximum (FWHM) when the monochromatic aluminum source is used. One of the few disadvantages of using a monochromator is that it reduces overall x-ray flux, but improvements in electron collection and detector efficiency have made this a minor consideration on modern instruments. Regardless of the type of source used, a very thin aluminum window is placed after the source to remove Bremsstrahlung radiation and electrons from the x-ray beam; this is especially important for nonmonochromatic sources where the Bremsstrahlung radiation is not removed by the monochromator.

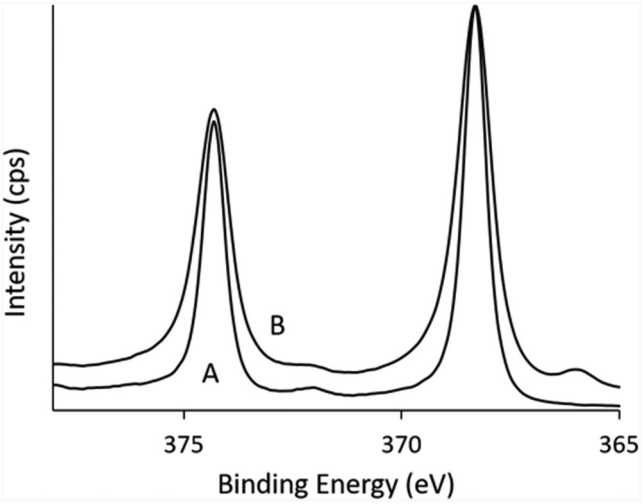

FIG. 8. XPS high-resolution spectra from a silver sample show the reduction in Ag 3d linewidth obtained from a monochromatic source (a) compared with a nonmonochromatic Mg source (b).

The x-ray source is designed to provide a high fluence of x-rays, since the number of electrons emitted is proportional to the x-ray source intensity; however, some samples can be damaged by high x-ray intensity.[58] Some indicators that sample damage may be occurring include visible sample color changes and spectral changes including peak broadening over time. Some materials are more susceptible to x-ray damage. For example, oxides are sometimes reduced, polymers can show changes in the C 1s peak shape and peak broadening, and thin films such as self-assembled monolayers have been shown to be susceptible to the loss of terminal groups.[59,60]

B. Electron lenses, analyzer, and detector

Between the sample and the analyzer are a set of electron optics called extraction lenses, and they serve several purposes. These lenses define the acceptance angle for collecting electrons emitted from the sample. Typically, a large acceptance angle is used to improve electron collection efficiency, although there are experiments for which lower acceptance angles are preferred (angle resolved XPS). On some systems, extraction lenses can also control the area of the sample from which electrons are collected, thereby enabling small spot analysis. Both angle resolved XPS and small spot analysis are described in more detail in Sec. VIII.

Energy resolution in XPS is limited by the energy of the electrons being detected, with better energy resolution achieved at lower electron energies. As a result, the energy of the electrons traveling to the analyzer is usually retarded or reduced by the extraction lenses to a specific user defined energy, called the pass energy, before entering the analyzer. The pass energy affects both electron throughput and resolution. Smaller pass energies result in better spectral resolution, but with fewer electrons detected, and are typically used for high resolution scans. In contrast, higher pass

energies are used for survey scans, where resolution is not important, because they can offer more electron throughput.

Two main types of analyzers were developed for XPS systems: cylindrical mirror analyzers and concentric hemispherical analyzers. Over time, the concentric hemispherical analyzer design proved to have better performance with respect to energy resolution and eventually throughput and is now used in all commercial XPS systems. The concentric hemispherical analyzer consists of two hemispheres as shown in Fig. 7(a). Voltages are applied to the hemispheres, with the outer hemisphere being more negative than the inner hemisphere. The electrons enter the analyzer through a slit, and only electrons with a specified energy will be able to travel through the analyzer. Electrons with higher energies will collide with the outer hemisphere and electrons with lower energies will collide with the inner hemisphere. The voltages on the hemispheres can be adjusted to allow electrons of different energies to pass through the analyzer. The analyzer resolution is determined by the radius of the analyzer, with larger radius analyzers providing better energy resolution. Many factors affect the energy resolution that can be achieved (source linewidth, analyzer radius, etc.), but modern instruments can achieve an energy resolution of less than 0.5 eV FWHM on the Ag $3d_{5/2}$ peak.[27,61]

All detectors used in XPS instruments are types of electron multipliers. Often multiple detectors are placed along the exit slit of the analyzer to collect more electrons; 2D position sensitive detectors are also available for either imaging or higher collection efficiency. More information on detectors can be found in the literature.[62]

C. Other features and options

While the above items (source, extraction lenses, analyzer, and detector) are required for any XPS, there are many other available options, and experiments utilizing these options are discussed in this article.

XPS systems are commonly equipped with some type of sputtering gun. Older systems routinely had just Ar^+ ion sources, which often cause sample damage. Newer systems offer more gentle sputter sources such as C_{60} or gas cluster ion sources (GCISs), commonly with argon clusters.

XPS imaging and small spot spectroscopy are also options. There are two main methods in which this is achieved. The first method reduces the size of the x-ray source to probe a smaller area on the sample. The second method retains a large x-ray source spot on the sample and controls the area from which electrons are collected with the electron optics.

Ultraviolet (UV) sources are offered as an option to enable ultraviolet photoelectron spectroscopy (UPS), which probes the Fermi level and energy levels just below Fermi. Commonly, a He source is used, and these sources can be operated to maximize the output of the He I (21.2 eV) or He II (40.8 eV) lines.

Additionally, sample heating and cooling are available from many vendors, often only in the analysis chamber, but sometimes also in the sample loading chamber. A resistive heater can produce sample temperatures over 500 °C, and liquid nitrogen cooling can reduce the temperature below −100 °C. Many applications have resulted from this capability.[63,64]

IV. SAMPLE PREPARATION AND MOUNTING

The allowed sample size will depend on the instrument configuration, but generally samples that are $10 \times 10\,mm^2$ and less than 10 mm tall should fit into the chamber. Because samples are analyzed in UHV, the samples must be vacuum compatible. This typically limits samples to solids, powders, and thin films, although high vapor pressure or even liquid samples can sometimes be analyzed when cooled or frozen in the chamber.[65] Instruments that can analyze samples at near ambient pressure are discussed in Sec. VIII. Some samples that are porous or polymer based will tend to incorporate volatile materials and then outgas in the UHV environment. It is recommended that the volatiles are first removed by extended pumping in a vacuum station prior to analysis.

For conducting or semiconducting samples, it is important to make electrical contact to the surface of the sample. Metal sample holders are provided for each system, and typically samples can be mounted with metal clips to ensure electrical contact. Double sided carbon tape is often used to adhere samples to the sample holder, and both carbon tape and indium foil are commonly used for mounting powder samples. Sample handling information for specific material types, such as polymers[66] and nanoparticles[67] have recently been published, and more detailed summaries are available.[68,69]

XPS can detect submonolayer coverages, so sample handling is very important! Gloves should be worn and metal tweezers used to handle the sample ***without contacting the area to be analyzed***, since studies have demonstrated contamination due to fingerprints and gloves.[70,71] Samples should be stored and transported in a way that does not introduce surface contamination. Fluoroware, glass, aluminum foil, or copier paper are all relatively clean containers for storing samples. As an example, silicon is a common contaminant that can come from many sources including the inserts in lids on glass jars, plastic bags, dessicators that use vacuum grease seals, plastic syringes with silicone lubricant, and sticky elastomer gel based sample holders. If unexpected elements are found on a sample, users are advised to examine anything the sample may have encountered. Both ASTM International and the International Standards Organization have published a number of recommendations for sample handling.[72–76]

Many samples of interest will oxidize rapidly in air, and methods have been developed to accommodate these samples. A sample fracture system can cleave the sample in vacuum to expose a fresh surface not exposed to ambient conditions. Many laboratories have also developed ways to transfer samples from a glovebox to the XPS chamber without exposure to air. Sometimes, the glovebox is directly attached to the XPS chamber,[77] but, more typically, samples are loaded onto the XPS sample holder in a glovebox, transported in an air-tight container to the XPS laboratory, and loaded without exposure to air. A simple way to do this is to enclose the sample loading port with a glove bag purged with nitrogen.

While sputter cleaning the surface can remove sample oxidation and/or contamination, it is not always recommended because the sputtering process (especially with an Ar^+ beam) often causes significant sample damage and changes in chemical state. Newer systems with argon cluster ion guns are more successful at cleaning polymer surfaces without sample damage as discussed in Sec. VIII. These more gentle sputter systems have also been shown to reduce

the extent of metal oxide reduction for materials like TiO_2 during sputtering.[78]

V. DATA ACQUISITION

A typical data acquisition sequence includes a survey spectrum to determine the elements present in the sample and high-resolution spectra of the elements of interest to determine peak shapes and chemical shifts. Data collection typically takes 30–60 min per sample depending on the number of high-resolution scans and the concentrations of those elements in the sample. There are several decisions that a researcher makes in the preparation for acquisition including the source to use, scan parameters, which lines to analyze, and whether to use the charge neutralizer.

A. X-ray source

The choice of which x-ray source to use will affect the transitions that can be observed, the spectral resolution that can be achieved, and the depth of analysis. While there are many theoretically available x-ray sources, most often a researcher is limited to the sources available on the XPS system being used. Since most instruments have Mg and Al sources, we will focus the discussion on a comparison of these sources.

Mg and Al sources have similar energies (1253.6 and 1486.6 eV, respectively), so there are not many differences in the transitions observed with these two sources. A few elements have transitions that can only be observed with the higher energy Al source including As 2p (1324 and 1359 eV) and Mg 1s (1303 eV). If there is a known overlap between an Auger line and a photoelectron line with one source, using a different x-ray source will move the Auger peaks and resolve this spectral overlap. For example, Ga has an Auger peak at 281 eV which often overlaps with the C 1s peak when an Mg source is used, whereas analysis with an Al source moves that Auger peak to 514 eV. If the system has a monochromatic Al source and spectral resolution is important, the monochromatic source will provide much better spectral resolution as demonstrated in Fig. 8. If determining the presence of a trace element is important, and spectral resolution is not a factor, then a nonmonochromatic Mg source can provide more x-ray flux and thus higher overall photoemission intensity for trace element detection.

In the case of Mg and Al sources, the depth of analysis is similar with only ~1 nm difference, so this is often not a factor in deciding which source to use. On systems equipped with monochromatic Al and Ag sources, the depth of analysis is a more important factor in choosing which source to use. Acquiring data with two sources, such as Al and Ag, or Al and Cr, provides a form of nondestructive depth profiling.

B. Scan parameters

Scan parameters including pass energy, step size, and dwell time are user controlled and need to be set appropriately to collect quality data. These parameters will vary for the acquisition of survey and high-resolution spectra, and from instrument to instrument. Survey spectra require high electron throughput, but spectral resolution is not a priority, and, therefore, a large pass energy is used. Survey data are often collected in larger steps (~0.5–1 eV), and relatively low dwell times are used. When high-resolution scans are acquired, more importance is placed on spectral resolution to discern subtle changes in the peak shape. As a result, a lower pass energy, smaller step sizes (~0.1 eV), and longer dwell times are used.

C. High resolution lines to scan

The user must also decide which lines to use for high-resolution scans. Most often, the highest intensity peak for a given element is used, as it is the easiest to detect, and will have the most reference data for comparison. But, in some cases, the most intense peak may have an interference from another peak or may not show as large a chemical shift as a less intense peak. The chemical shift between Ga and Ga_2O_3 is only about 1 eV for the Ga 2p line but is more than 2 eV for Ga 3d. If the signal intensity from the Ga 3d is sufficient, the data from that line may be more conclusive to separate these two chemical states than the data from the Ga 2p line. It may be necessary to collect data from multiple photoelectron lines (or from photoelectron and Auger lines) to provide a valid interpretation of the chemical state.

D. Charge neutralization

Insulating samples can charge during XPS analysis causing unwanted peak shifts and distortions in peak shapes.[78–84] Even though the incident x-rays are not charged, the emission of photoelectrons and Auger electrons may cause the sample to acquire a positive charge. For conducting and semiconducting samples, an electrical contact is made to the surface of the sample, and the sample holder is grounded. This connection to ground allows the electrons lost due to photoemission to be replaced, but this strategy does not work well for insulating samples. When a sample starts to charge positively, it becomes more difficult to remove the subsequent electron, and the binding energy of that electron is increased causing peaks to shift to higher binding energy. In addition, charging often affects different parts of the sample differently (termed differential charging)[85,86] and can lead to effects like peak broadening and the addition of new peaks or shoulders, which can be quite dramatic as shown in Fig. 9. Charging is less prevalent with nonmonochromatic sources, as the large flux of x-rays strikes the aluminum window separating the x-ray gun from the chamber, the sample holder, and the spectrometer surfaces, thereby producing secondary electrons which can act as a type of built in charge neutralizer.

Often, the use of a charge neutralizer can eliminate the effects of charging observed in the spectrum. Charge neutralizers are typically located above the sample in the vacuum chamber and they supply a source of low energy electrons (1–5 eV) or ions (<5 eV). Commonly the peak height, width, and shape are monitored while adjusting the charge neutralizer parameters to determine the best set of conditions to use. Ideally, the parameters that produce the narrowest peaks are used, and often data are acquired under a number of charge neutralizer conditions to determine the best parameters. Figure 9 shows the Cl 2p peaks from an NaCl sample acquired with different charge neutralizer conditions. After charge neutralizer conditions had been optimized and the effects of charging had been eliminated, a well resolved Cl 2p doublet is observed [Fig. 9(a)], but Figs. 9(b)–9(d) illustrate how peak broadening, peak shoulders, and additional peaks can be observed when samples are

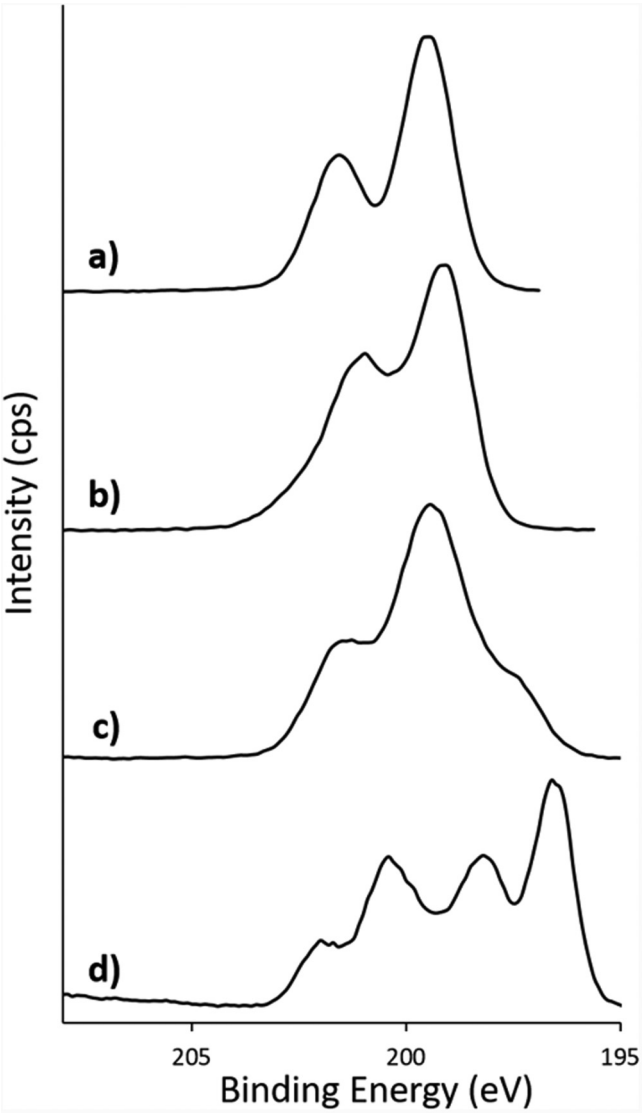

FIG. 9. Cl 2p high resolution spectra from a NaCl sample were obtained using different charge neutralizer conditions. The examples show (a) absent, (b) slight, (c) moderate, and (d) severe charging.

not properly neutralized. In the case of Fig. 9(d), if the user assumed that the sample was not charging, they would likely conclude that there were multiple types of Cl present in the sample since it appears that multiple Cl 2p doublets are present. Obviously, care must be taken when interpreting data, especially when charging is suspected, and often data from other elements in the same sample are also consulted to determine if charging has been eliminated. The performance of a charge neutralizer is commonly determined by analyzing PET. The FWHM of the O—C═O peak [peak labeled C in Fig. 4(b)] is commonly reported, with smaller FWHM indicating better performance.[84]

Caution Box 3:

Surface and near surface charging can impact spectra in ways that surprise many users. Charge accumulation around interfaces can set up dipole layers that shift the measured BEs. If a "partially" conducting sample is both grounded and subject to electrons or ions from a charge neutralization system, an electric field can be established across the sample that may shift peak energies in parts of the sample or cause peak distortion.[82] In this case, different parts of the sample may be at different potentials, and disconnecting the ground connection while using the charge neutralizer may produce better results.

Even with the proper use of a charge neutralizer, peak shifts are frequently observed, making comparisons to other reference data difficult. To correct the energy scale, some sort of internal standard with a known energy position is needed. Almost all surfaces have some level of carbon contamination present from exposure to atmosphere, commonly called adventitious carbon, and the lowest binding energy C 1s peak (corresponding to graphitic or CH_2 like carbon) is often used as the internal standard for the purposes of energy calibration. Unfortunately, an appropriate binding energy of this peak is uncertain and values ranging from 284.6 to 285.0 eV have been used. At least in part this is because the true nature of the adsorbed carbon varies. The impact of carbon source variations, interactions with different substrates, and the coupling of the adsorbed layer to the substrate limit the validity of using the C 1s peak as an accurate "universal" reference, and this has been discussed in the literature.[84,87] Regardless, it is the easiest and most commonly used form of charge correction in XPS. Once the appropriate shift for the C 1s peak is determined, the data for the other elements in the same sample are corrected by the same amount, with the assumption that they are charging to the same degree. The method for energy calibration should always be reported in the experimental section of a paper containing XPS data so that other researchers can make peak position comparisons.

VI. PEAK IDENTIFICATION

Each element has a unique XPS spectrum based on the energy levels for that element, and any transition with a binding energy less than the x-ray source energy should be observed in the XPS spectrum. To help with identification, reference books are available with spectra for each element,[24–38] and it is recommended that a user have access to one of these references to help with peak identification. These books contain the energies for each expected photoelectron peak, selected data on chemical shifts, expected peak splitting, and peak shapes as discussed below. Software analysis packages also have libraries of peak positions, but often chemical shifts, relative peak intensities, and peak shapes are not included in these libraries, and the reference books are still very helpful.

All XPS lines except those from the s orbitals occur as doublets due to spin–orbit coupling. Doublets are commonly notated with the j quantum number as a subscript. For example, the Ti 2p doublet consists of the Ti $2p_{1/2}$ and the Ti $2p_{3/2}$ peaks. The intensity ratios of the peaks in a doublet are also defined by these j quantum numbers.

Relative intensities are determined by 2j+1. For the Ti 2p peaks, the ratio of the heights should be 2:1 for the Ti $2p_{3/2}$ and Ti $2p_{½}$ peaks, respectively (2*3/2 + 1 = 4 and 2*1/2 + 1 = 2, therefore, the ratio is 4:2 or 2:1). Intensity ratios for the d and f doublets can be similarly calculated as 3:2 for d orbitals and 4:3 for f orbitals, respectively. Sometimes, the peak separation between the doublet is too small to resolve with the XPS experiment, as with the Al 2p peaks, but again a good reference book will indicate this.

There are additional types of peaks that appear in spectra that can easily confuse novice XPS users.[88–91] As mentioned above and shown in Fig. 3, satellite peaks occur when a sample is excited with x-rays of more than one energy, resulting in additional XPS peaks at lower binding energies. These satellites can be eliminated entirely with the use of a monochromatic x-ray source.

Shakeup peaks, also called loss peaks, result from a de-excitation process, where the outgoing core electron interacts with a valence electron and excites it to a higher energy level. The core electron kinetic energy is reduced by some quantized amount, and the result is a peak which occurs at a few electron volts higher binding energy than the core level XPS peak. In Fig. 10(a), the

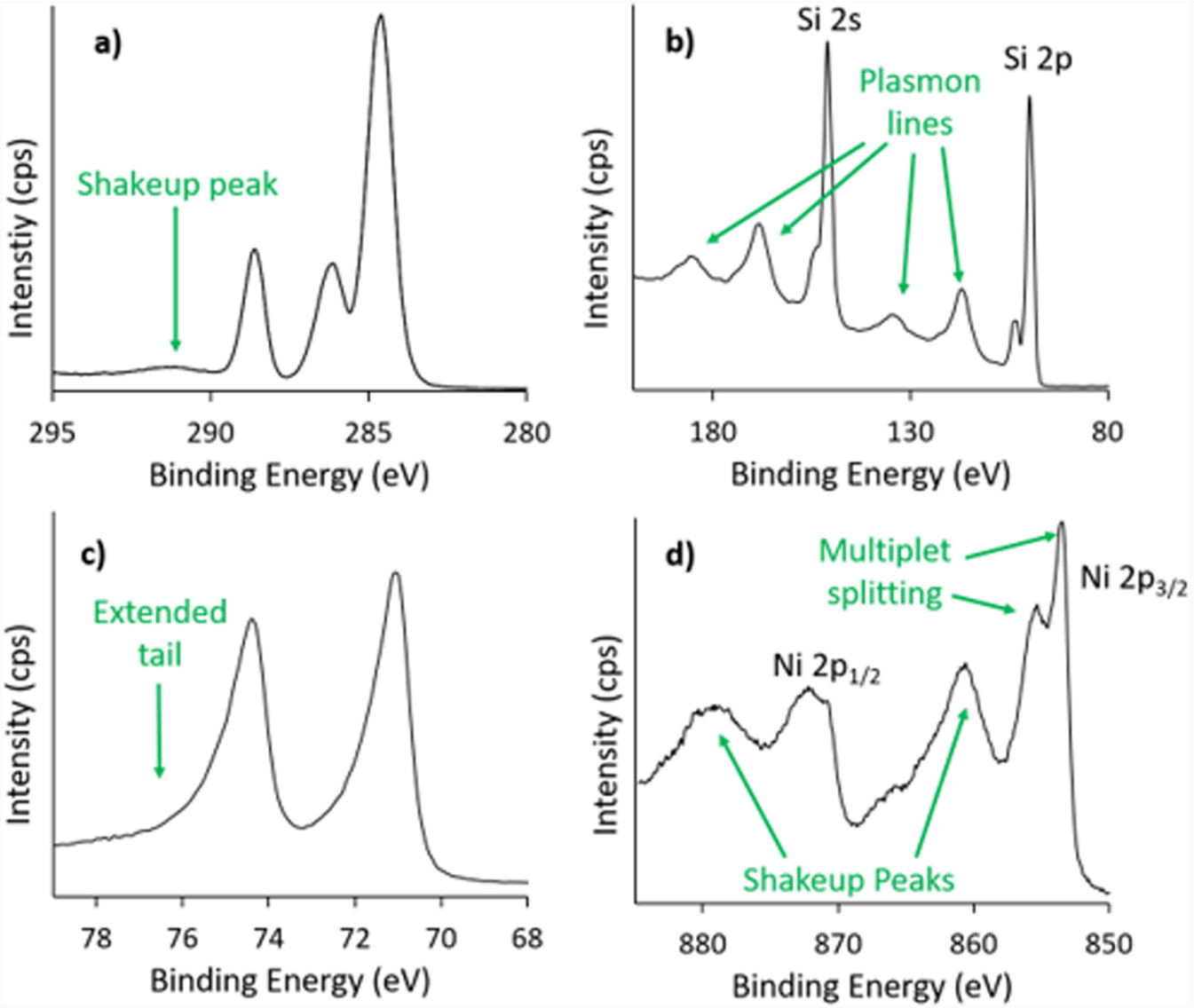

FIG. 10. Examples of shakeup peaks and multiplet splitting include (a) shakeup peak in the C 1s spectrum of PET due to the π→π* transition, (b) shakeup peaks due to the excitation of plasmon lines in Si, (c) tailing on a metallic peak for Pt 4f, due to shakeup excitations into a continuum of states above the Fermi level, (d) multiplet splitting and shakeup peaks in the Ni 2p spectrum from NiO.

shakeup peak in the C 1s line from the analysis of PET is due to the $\pi \rightarrow \pi^*$ transition, which appears at 6.6 eV higher binding energy than the primary peak. Another example of an energy loss process is the excitation of plasmons in a metal. The resulting plasmon loss lines are observed as characteristic peaks as shown for silicon in Fig. 10(b). Transitions for metals sometimes exhibit an asymmetric peak shape with a tail on the high binding energy side of the peak. Metals have many closely spaced unfilled states just above the Fermi energy, and excitation of valence electrons to this continuum of states can occur. As a result, a tail is observed instead of a discrete peak. An example of this is shown in Fig. 10(c) and is important to consider when peak fitting.[16] Shakeoff peaks are similar to shakeup peaks, but instead of exciting an electron to a higher state, the electron is ejected from the atom.

Multiplet splitting of core level peaks occurs when there are unpaired electrons in the valence levels and often results in unexpected peak splitting. This affects the s orbitals of some transition metals [Mn(II), Cr(II), Cr(III), Fe(III)] and also can be observed for some p and d orbitals as well. Figure 10(d) shows an example of multiplet splitting for Ni 2p in an NiO sample, which also exhibits shakeup peaks as indicated.

While the inexperienced user may have trouble differentiating between various types of satellite peaks, shakeup peaks and multiplet splitting, it is important to remember that many basic XPS reference books will indicate when peak shapes for a given element are not simple doublets/singlets as expected. Sometimes, this is all the user needs to confirm that their results are normal for a particular element. At other times, the data in the reference book may be the first step in a deeper literature search. The NIST and Surface Science Spectra databases can provide very helpful information.[33,35]

VII. DATA ANALYSIS

A. Qualitative analysis

Commercially available software packages for data reduction are available, but each instrument manufacturer also provides their own data reduction software as well. All of these software packages offer similar features for analyzing data, including element libraries, baseline subtraction, peak fitting, energy calibration, and quantification.

The first step in analysis of XPS data is to assign all the peaks in the survey spectrum. Knowing something about the elements present in a sample can be helpful in starting this process but is not required. Often, it is easiest to start with the largest peak in the survey spectrum and determine its assignment first, because that same element may also be responsible for other less intense peaks as well. If it is suspected that a sample contains Ag, for example, the peaks displayed in Fig. 3 (Ag 4d, Ag 4p, Ag 4s, Ag 3d, Ag 3p, Ag 3s, Ag Auger) should be present with the same relative intensities as shown. If they are not, then perhaps Ag is not actually in the sample. When transitions originating from p, d, or f orbitals are present, the peaks of the doublet should match the known energy separation and have the correct relative intensity of the peaks in the doublet. Some doublets will be resolved in the survey spectrum, but high-resolution spectra may help with this part of the identification. Auger electron transitions often occur as a series of peaks as shown for silver in Fig. 3, and these series of peaks should generally match that observed in the spectrum. Remember, if a nonmonochromatic source is used, satellite peaks will be present. Very intense plasmon peaks can also sometimes be observed, but often shakeup peaks and peaks due to multiplet splitting will not be resolved enough to observe in the survey spectrum. Utilizing all of these clues makes it possible to identify the elements present in a survey spectrum.

Caution Box 4:

Care must be taken with automatic peak finder features available in many software packages. Errors in identification can occur when the peak finder indicates the presence of an element based only on a single peak and not the entire series of peaks for that element. It is recommended that users double check the results from automatic peak finders to ensure that the results are reasonable.

To compare binding energies with any reference texts, two things must be done: (1) the energy scale needs to be calibrated to ensure its linearity and (2) the energy scale may be adjusted based on the position of a reference peak. At least two peaks are needed to calibrate the energy scale, and ISO, ASTM, and various vendors provide methods for instrument calibration. Most of the approaches involve measuring and adjusting the binding energy scale by using lines at high and low binding energies. Commonly, the Au $4f_{7/2}$ line at 84.0 eV and the Cu $2p_{3/2}$ line at 932.6 eV are used for this purpose (ASTM E2108 and ISO 15472).[92,93]

Once the BE scale is calibrated, the energy scale may be adjusted with a peak with a "known" binding energy, especially if there is a concern about peak shifts due to surface charging. Carbon contamination is present on almost every surface analyzed by XPS, and the C 1s peak is the most common way to reference the energy axis. As mentioned earlier, the lowest binding energy C 1s peak is typically shifted to an energy between 284.6 and 285 eV, and then all other elements in that sample are shifted by the same amount. Other elements, if well characterized, can also be used. Even with all of the faults associated with using C 1s, it is by far the most commonly used method for energy correction. In all cases, it is assumed that the element used for calibration is undergoing the same charging behavior as the rest of the sample. If this is not true, then that element may not provide a good energy reference.

Once the energy scale is calibrated and adjusted, it is possible to make accurate binding energy measurements to identify chemical states for specific elements. Many states exhibit a chemical shift that is sufficiently different (>0.2 eV shift) from other states to aid in identification. Reference books are a good place to start to identify the chemical environment around the element in question, but a user should consult multiple sources or even run standard samples on their own instrument to conclusively assign peaks.

B. Background subtraction and peak fitting

Before doing any peak fitting or quantitation, the peaks in the survey and/or high-resolution spectra must be fit with a background.

When high-resolution spectra are available, they will typically give better results (the data are acquired at higher resolution and often a better signal to noise ratio is observed), and are preferred to survey data for quantitation, and especially for peak fitting. Many background options are available within commercial software programs,[15] but the most common backgrounds are linear, the Shirley background[94] [as shown in Fig. 11(a) for a W 4f peak with multiple states], and the Tougaard background. The linear background simply fits a straight line to the two data points chosen as the endpoints of the background range. Remember that there are electrons generated in a sample that undergo inelastic scattering events and contribute to the background signal [electrons labeled B in Fig. 5(a)], and the steps in the background [Fig. 5(b)]. Often, a linear background is a very poor approximation of the actual background shape. The shape of both the Shirley and the Tougaard backgrounds is not linear. The Shirley background assumes that the change in the background signal is proportional to the peak intensity above the background at a certain binding energy, while the Tougaard background models the inelastic scattering that the electrons undergo. A full discussion of the advantages and disadvantages of the Shirley and Tougaard backgrounds is beyond the scope of this text, but the importance of choosing appropriate end points for each background and the results of different backgrounds on quantitative results have been discussed elsewhere.[12,15,95,96]

Peak fitting may be required to determine if multiple chemical states are present and to determine the relative concentrations of each component. Peak fitting must be done carefully! It is very easy to add peaks to improve the overall fit, but users should make sure that they can justify the components they are adding. Peak fitting should be a part of a comprehensive and self-consistent model of the sample that takes all elements into account.[16,87,97]

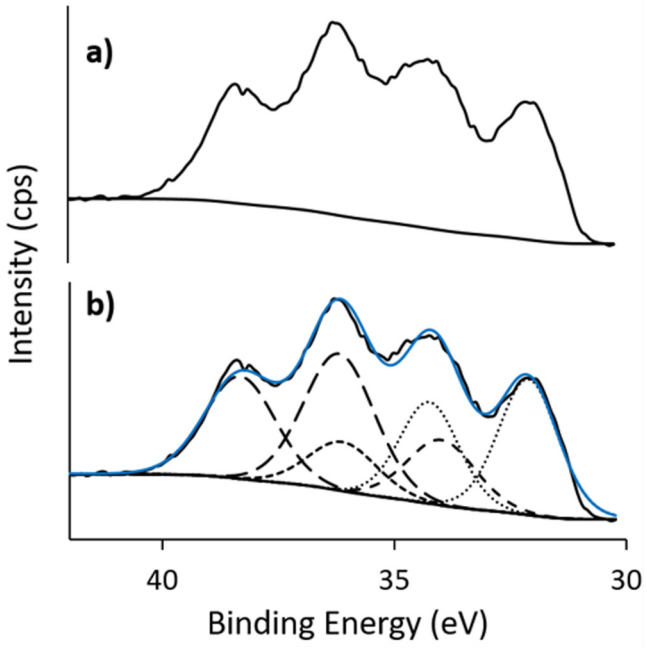

FIG. 11. Data analysis often involves fitting a baseline to the data and peak fitting. A Shirley baseline is shown in (a), and three doublets are used to fit the W 4f peak in (b).

Caution Box 5:

Peak fitting is perhaps the most common place where mistakes in analyzing XPS data occur. It is not unusual in the experience of the authors for a researcher to want to reproduce the poor peak fitting they see in published papers. Common mistakes include not fitting p, d, and f peaks with doublets, interpreting shakeup or satellite peaks as additional chemical species, and trying to infer the chemical species present from inconclusive peak fitting of broad peaks.[97]

A simple example of peak fitting is shown in Fig. 4(b) for the C 1s peak from PET. Since the data are for an s-orbital, there is no peak splitting and singlets can be used. In general, the peak widths should be similar for the peaks within a fit and should not exceed 1.5–1.8 eV. The reported binding energies for C═C, C—O, and C═O are consistent with the positions of the peaks obtained from peak fitting and help to confirm the assignment of the peaks. The areas under the peaks can be used to quantify the different components as described in the quantification section below.

Peak fitting can be more complex as shown in Fig. 11(b). In this example, an aluminum metal top contact was deposited by thermal evaporation on a layer of WO_3 to investigate changes in the WO_3 during the deposition of the top contact. Interfacial changes in chemistry can significantly affect the ability of charges to move across an interface in electrical devices, and the combination of surface sensitivity and sensitivity to chemical environment makes XPS uniquely qualified to address these questions. Before aluminum deposition, the W 4f region showed the expected W 4f doublet at peak positions consistent with WO_3 (data not shown). After 3 nm of aluminum deposition, the curve in Fig. 11 was obtained. To understand the chemical states present, peak fitting was required, and the W 4f peak was fit with three doublets. When peak fitting with doublets, the correct energy separation between the peaks in the doublet and the correct height ratio must be used for valid fitting. Software packages allow users to constrain or link certain peaks together to apply these rules to doublet peaks. This analysis showed the formation of multiple reduced tungsten species as a result of the aluminum deposition.

C. Quantitative analysis

An important feature of XPS is the ability to determine atomic concentrations without the use of standards. After baseline subtraction, the area under a peak can be measured, but raw areas alone cannot be used to determine relative concentrations. Instead, a sensitivity factor that is specific for each transition must be considered as described in Eq. (5),

$$C_x = (I_x/S_x)/(\Sigma(I_i/S_i)), \quad (5)$$

TABLE IV. Sensitivity factors for some commonly analyzed elements (Ref. 102), derived and reprinted with permission from Scofield, J. Electron Spectrosc. Rel. Phenom. **8**, 129 (1976). Copyright 1976, Elsevier.

Element	Sensitivity factor	Element	Sensitivity factor	Element	Sensitivity factor
C 1s	1.00	Ca 2p	5.13	Ag 3d	18
N 1s	1.77	Cr 2p	11.5	In 3d	22.4
O 1s	2.85	Ni 2p	21.1	Sn 3d	24.7
F 1s	4.26	Ni 2p 3/2	13.9	Hf 4f	7.95
Na 1s	7.99	Ni 2p 1/2	7.18	Ta 4f	9.07
Al 2p	0.5735	Cu 2p	24.1	W 4f	10.3
Si 2p	0.865	Ga 2p	31	Pt 4f	15.9
Cl 2p	2.36	Mo 3d	9.74	Au 4f	17.4

where I is the peak area or intensity, S is the sensitivity factor, C is the atomic concentration, x is the species of interest, and i represents all possible species. A higher sensitivity factor indicates that the transition is easier to observe (has a stronger signal) than a transition with a low sensitivity factor. Table IV shows sensitivity factors for some commonly analyzed elements and there are many tables of sensitivity factors.[98–102] For example, if a survey spectrum showed the presence of both gold and carbon, and the Au 4f and C 1s peaks had the same intensity, there would be ~17.4 times more C than Au ($S_{Au\ 4f}/S_{C\ 1s} = 17.4/1$).

Sensitivity factors also take into account some instrument specific sensitivities (analyzer and detector), so you will find that the sensitivity factors used by different XPS vendors will vary slightly. The sensitivity factors shown in Table IV are referenced to the C 1s peak with a value of 1 (although some reference texts will use the F 1s peak as this reference),[98] and they range by a factor of ~50 over most of the periodic table. The detection limit for XPS is typically quoted as ~0.1–1 atomic percent but will depend on the sensitivity factor of the trace element and the sample matrix.[25] In actuality, detection limits can range from 0.003 atomic percent up to 30 atomic percent, and they have been predicted for all elements in all elemental sample matrices.[103] An accuracy of ~±10% is quoted for XPS quantitation,[104] but in reality, this depends heavily on the peak shape, the ability to accurately fit the background, and the correct use of relative sensitivity factors, and can range from 4% to 15% depending on these factors.[13,87] It is worth noting that the technique is much more precise than it is accurate, and XPS is very good at detecting small relative changes in concentration at less than 1%.[12]

Sometimes, overlaps between a peak of interest and other peaks will prevent the easy determination of peak area for the peak of interest. In some cases, peak fitting will allow the user to separate out the area contributions from each element, and quantitation can occur based on this peak fitting. In other cases, perhaps one peak from the doublet is well resolved. In that case, the concentration of that element can be determined by using a modified sensitivity factor. An example of this is shown in Table IV for Ni 2p, where the sensitivity factors for Ni 2p (both peaks), Ni $2p_{½}$, and Ni $2p_{3/2}$ are shown. In Fig. 4, the C 1s peak from PET was fit with three components. In this case, calculating the concentrations of the three different types of carbon is obtained by simply comparing the relative area under each peak, because the sensitivity factors are the same (they are all C 1s peaks). However, to calculate the relative atomic percentages of carbon and oxygen, the sensitivity factors would need to be considered. Software programs make these calculations easy for the analyst. Numerous guides for data recording and analysis to improve reproducibility are available from the ASTM International and ISO.[105]

Remember that XPS is most sensitive to the elements at the very surface of the sample, and these atomic concentration calculations assume that the sample is homogeneous over the depth and area analyzed. If the sample is layered within the top ~10 nm, then care should be given to interpret quantitative data. The concentration from the top layer will be overestimated relative to the concentration of layers below. Many samples have layered structures, especially at the surface due to surface oxidation.

XPS data can be used to estimate the thickness, d, of an overlayer "A" on top of a substrate "B" using Eqs. (6) and (7),

$$I_A = I_A^{\infty}(1 - e(-d/\lambda^A{}_{imfp}(E_A)\cos\alpha)), \quad (6)$$

$$I_B = I_B^{\infty}(e(-d/\lambda^A{}_{imfp}(E_B)\cos\alpha)), \quad (7)$$

where I_A and I_B are the intensities from the overlayer and substrate, respectively, and I_A^{∞} and I_B^{∞} are the intensities from pure A and pure B. The term $\lambda^A{}_{imfp}(E_A)$ is the IMFP or attenuation length of electrons traveling through A, with kinetic energies characteristic of the electrons originating from A. Likewise, $\lambda^A{}_{imfp}(E_B)$ is the IMFP or attenuation length of electrons traveling through A, with kinetic energies characteristic of the electrons originating from B. The term α is the angle of emission of electrons as described in the next section on angle resolved measurements. These calculations require measurements from pure A or B and assume that the layered sample is flat and homogeneous within each layer.

Caution Box 6:

There are two types of relative sensitivity factors (RSFs): empirical RSF determined with the aid of reference materials and theoretical RSF.[13] Theoretical RSF values will account for all of the area produced by the electrons from a particular orbital, including the main photoemission peak, but also all satellite, shakeup, shakeoff, and multiplet splitting lines as well. Some of these features can be quite far from the main line [as for the Si plasmon lines in Fig. 10(b)], and thus the experimental data acquisition should account for this wider scan to capture all of the relevant features. Empirical RSF values often only include the intensity from the main photoemission line. Users should consult the instrument/software vendor to determine the type of RSF values used to acquire and analyze data accordingly.

VIII. VARIATIONS ON THE TECHNIQUE

A. Angle resolved XPS

While XPS is a very surface sensitive technique, there are advantages to modifying the surface sensitivity. One way to do that is by changing the orientation of the detector to the sample surface normal (α), referred to as the angle of emission.

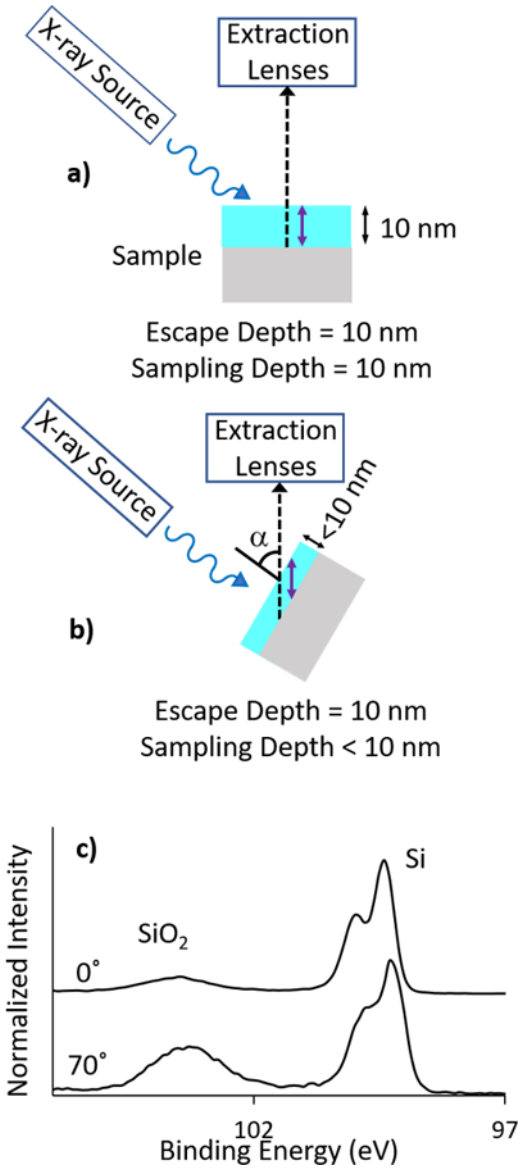

FIG. 12. Tilting the sample is an easy way to change the depth of analysis in XPS. While the escape depth is constant in both (a) and (b), tilting the sample increases the angle of emission, α, and results in a smaller information depth. Figure (c) shows the relative difference in the intensities of Si and SiO_2 peaks at two different emission angles. At 70°, the increased relative intensity of the SiO_2 component indicates that it is present on the surface of Si.

Figure 12(a) and 12(b) show that the angle of emission can be changed by simply tilting the sample. When the sample is untilted ($\alpha = 0°$), the escape depth (shown by the double pointed arrow in the top layer of the sample) and the information depth or sampling depth (shown by the 10 nm blue portion of the sample) are the same. When the sample is tilted, as in Fig. 12(b) ($\alpha = 70°$), the escape depth does not change since this is a physical parameter defined by the electron energies and the material they are traveling through. However, the path they must take to reach the detector does change, and as a result, the sampling depth is reduced. In this way, a larger angle of emission enhances the signal from the surface, and this technique is referred to as angle resolved XPS (ARXPS). Analysis at several angles can provide a nondestructive "depth profile" of the top ~10 nm.[106,107]

Figure 12(c) shows an example of the information this approach can provide. The Si 2p data from a silicon wafer with a native oxide show elemental Si lines at ~99 eV and Si(IV) lines from SiO_2 at ~103 eV. The original data, taken at 0°, do not indicate if this is a layered sample or if Si and SiO_2 are a homogeneous mixture. Comparison of the data at 0° with that at 70° shows a difference in the relative intensity of these two components. When a thinner layer of the surface is probed during the experiment at 70°, the SiO_2 component is higher in intensity relative to the Si component, indicating that SiO_2 is indeed a surface layer on top of Si. If it was a homogeneous mixture, the relative ratio of the two components should not change upon tilting the sample.

Any simple quantitative angle resolved XPS relying on Eqs. (6) and (7) assumes a flat sample surface, and flat layered samples that are homogeneous within each layer. Samples exhibiting surface roughness will exhibit different electron angles of emission and shadowing effects.[108] In addition, islands (buried or on the surface) also affect electron trajectories in ways that affect the quantitative XPS data especially for angle resolved XPS. These effects can be accounted for and modeled, but they complicate the analysis and often require software programs to extract reliable information.[109–112]

B. Depth profiling

In some cases, the user may want to probe deeper into the sample, and many systems are equipped with a sputter gun to physically remove material from the sample. Depth profiling by sputtering is a major application of secondary ion mass spectrometry (SIMS)[113,114] but can also be applied to XPS. In these experiments, XPS data are acquired, the sample is sputtered for a short amount of time, and then XPS data are acquired again. This procedure is repeated until the sputtering has probed to the depth of interest. Some sputtering experiments will probe hundreds of nanometers to micrometers into a sample and may take many hours to perform. Historically, Ar^+ has been the most commonly available sputtering source, and an example of data acquired from Ar^+ sputtering is shown in Fig. 13(a) for a Ta_2O_5 thin film on a Ta substrate. The depth profile shows the concentrations of tantalum and oxygen as a function of sputtering time and can provide a measure of the film thickness if the sputtering rate is known. Figure 13(b) shows how the Ta 4f high resolution peaks transition from a Ta_2O_5 doublet to a Ta doublet as the oxide film was sputtered away.

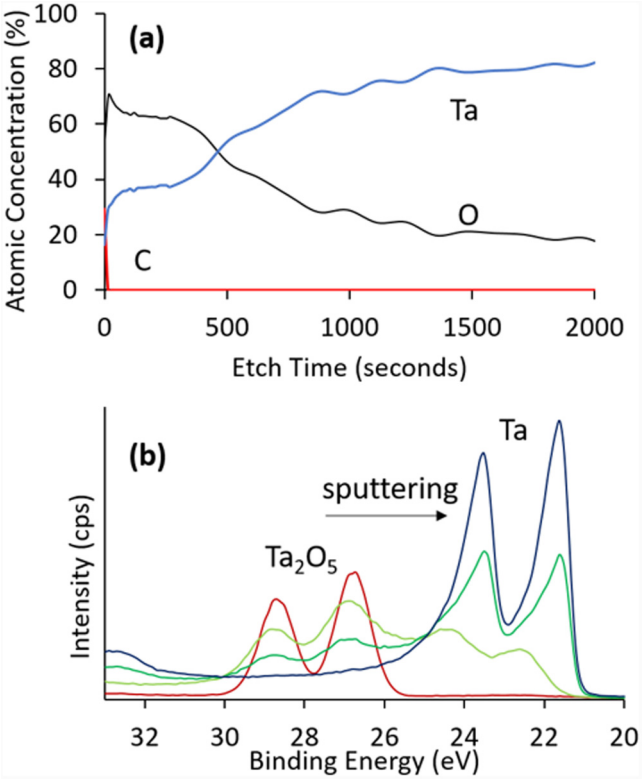

FIG. 13. Elemental depth profile of a Ta_2O_5 film (a) shows the presence of a thin carbon contamination layer, and a change in Ta and O concentrations as the Ta_2O_5 film is removed to expose elemental Ta. High resolution Ta 4f spectra (b) show the change in the peak position and peak shapes as the Ta_2O_5 oxidized layer is sputtered away.

Some caution needs to be used when sputtering samples with Ar^+ ions, since they physically damage the sample in a somewhat uncontrolled manner. Some atoms are more likely to be sputtered than others, a process called differential sputtering, and this can result in measured atomic ratios that are different from the actual atomic ratios in the original sample. In addition, the interaction between the sample and the ions can change the chemical state of the sample. For example, the metal in many metal oxides will be reduced upon Ar^+ sputtering (e.g., TiO_2 reduces to TiO),[115,116] and sputtering polymer samples without damaging them is almost impossible with an Ar^+ sputter gun. As a result, more gentle ion sources including C_{60}^+ and argon clusters have been developed. These sources are able to more successfully sputter many types of polymers without damage and have shown an ability to reduce the amount of metal oxide reduction that occurs as a result of sputtering in samples such as TiO_2.[78,117–120]

C. Small area/imaging

Typical analysis areas for XPS are on the order of hundreds of micrometers, but sometimes, it is advantageous to probe smaller areas on the surface.[121] There are two approaches to collecting electrons from a smaller spot size: lens defined and source defined. With lens defined analysis, the x-ray beam is not focused and irradiates a broad area. Electrostatic lenses in the electron extraction column restrict the region from which electrons are accepted. In a source defined system, the x-rays are focused to a small spot on the sample to limit the area irradiated. Typical small spot sizes range from 10 to 100 μm in diameter,[122] and reducing the spot size will require longer integration times to produce quality data.

XPS imaging is also an option on some systems, and different vendors have implemented different strategies to accomplish this by: (1) rastering a focused x-ray beam on the sample surface, (2) moving the sample under a stationary focused x-ray beam, and (3) using a large x-ray beam, but utilizing the extraction lenses to preserve the spatial resolution of the electrons and to produce an image at the detector. XPS imaging with spatial resolution of 1–3 μm has been achieved.[123]

Caution Box 7:

There is often confusion between the terms image resolution and analysis area. Often image resolution is measured by observing a material containing materials A and B separated by a sharp edge. The distance required for the signal from A to go from 84% to 16% (or other defined percentages) is defined as the image resolution. But, by definition, there is "spill over" of the signals at these edges. The result is that typically the instrument spatial resolution must be several times (~5×) smaller than the feature to be measured to assure that 90% of the XPS signal comes from only the feature of interest.[18,123]

D. Near ambient XPS

One of the limitations of XPS is the ultrahigh vacuum environment in which measurements are performed. This prevents the analysis of many surfaces under conditions in which they are typically used (ambient conditions or in solution). As a result, some manufacturers have developed near ambient pressure XPS (NAP-XPS), also called environmental XPS.[124,125] These systems allow operation at pressures up to 25 mbar or higher and enable the analysis of semivolatile liquids, samples with significant

Caution Box 8:

Near ambient and solution cell measurements can be quite useful and informative; however, there are many issues to consider to perform careful measurements and analysis. The relatively high pressure environment lowers signal intensities making it more difficult to measure trace elements. The gas environment of NAP-XPS also influences sample charging, which can cause peak shifting that varies with gas pressure. When this is observed, the determination of chemical states from these data should be avoided.

outgassing, and biological samples. Most vendors do this by differential pumping of the extraction lenses. In this way, the pressure is gradually reduced to $\sim 10^{-8}$ mbar as the electrons approach the analyzer. Other vendors have created NAP-XPS systems by using a capillary to deliver small amounts of gas to the area just in front of the sample, increasing the pressure locally at the sample surface, but keeping the overall pressure in the chamber low.

Another strategy is to build a thin sample cell that holds a small amount of gas or liquid.[126–130] However, fabricating a cell with a window that is thin enough so electrons can escape is extremely challenging. Window materials have included thin (5–15 nm) Si and SiN films, graphene oxide, and graphene sheets. Initial studies of liquids and the interior surface of the window material have demonstrated proof of concept of these designs. Major challenges include the low number of electrons that can escape these cells, and the analysis of surfaces submerged in liquids. Some work with these environmental sample chambers has also been done on synchrotron systems, where x-ray flux is higher, and x-ray energy is tunable.[131–133]

E. Valence XPS spectra and UPS

In the XPS spectrum, there are features at a low binding energy (less than 30 eV) due to the ejection of valence shell electrons. This region of the XPS spectrum is often referred to as the valence region, and it can lend additional information to an analysis.[134–136] For example, the C 1s spectra of polypropylene and polyethylene are identical, but differences in their valence region spectra allow for the two polymers to be distinguished by XPS.[27]

In addition, some XPS systems are also equipped with ultraviolet sources, most commonly a He-I source with an energy of 21.2 eV to enable ultraviolet photoelectron spectroscopy (UPS) experiments. This technique is the same as XPS but irradiates the sample with a UV source instead of an x-ray source. Since the energy of this source is low compared to x-ray sources, it can only eject valence level electrons with very low binding energies. The low energy of the UV source also makes this technique even more surface sensitive than XPS with only the top ~2–3 nm analyzed, and therefore, surface contamination can be even more problematic.

Figure 14(a) shows the UPS spectrum of Au. UPS spectra are essentially density of states diagrams with a focus on the energy levels just below the Fermi level.[137–139] UPS data can be used to determine the work function (energy between Fermi and vacuum) of a material and also the ionization energy, the energy between the vacuum level and the first valence level in a semiconductor (or the highest occupied molecular orbital, HOMO, in a molecule). The binding energy on the x axis is typically reported with respect to the Fermi energy (BE = 0 eV = Fermi energy). The Au spectrum in Fig. 14(a) shows a clear Fermi edge at 0 eV and occupied states just below the Fermi edge in the range of 2–7 eV. At close to 16 eV, the intensity suddenly drops. Electrons in energy levels with higher binding energies are not probed because the energy of the UV source (21.2 eV) is unable to eject those electrons. This portion of the spectrum is often called the secondary electron cutoff (E_{cutoff}).

Equations (8) and (9) describe how to determine the work function (Φ) of a material as described by the energy diagram in Fig. 14(b). In Fig. 14(a), E_{cutoff} was measured as 15.95 eV; thus, the work function can be calculated as 5.25 eV as shown in Eq. (9).

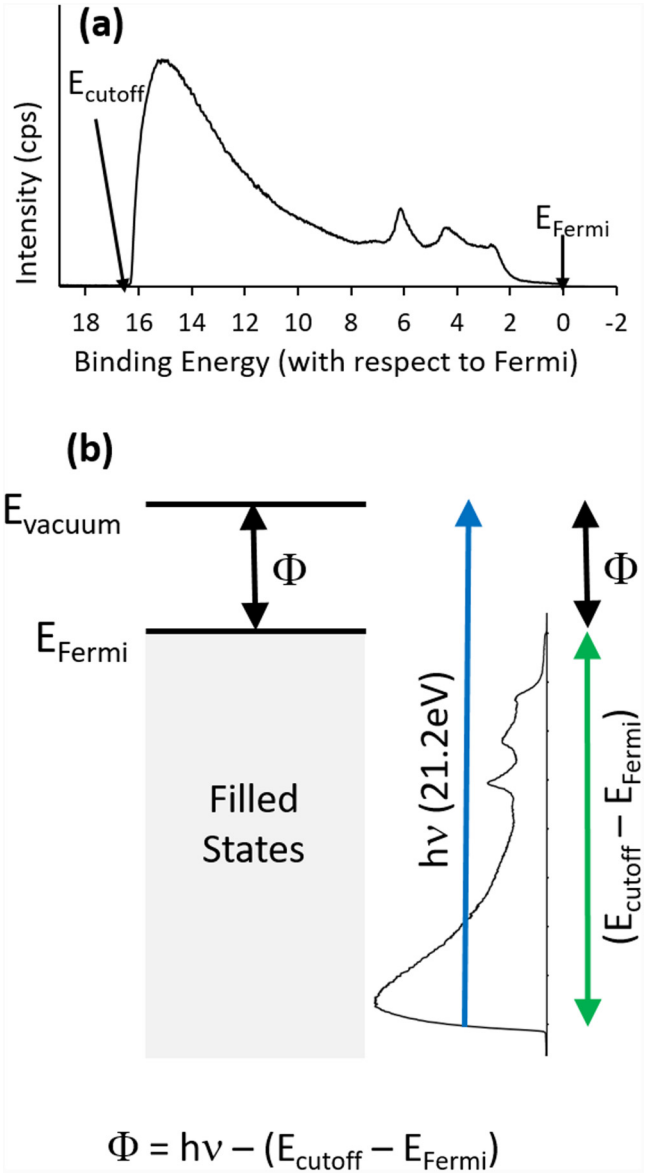

FIG. 14. (a) UPS spectrum for Au with the Fermi energy (E_{Fermi}) and the secondary electron cutoff (E_{cutoff}) indicated. (b) An energy level diagram shows how the UPS spectrum is a density of states diagram and illustrates how to calculate the work function.

$$\Phi = h\nu - (E_{cutoff} - E_{Fermi}), \tag{8}$$

$$\Phi = 21.2\,\text{eV} - (15.95\,\text{eV} - 0\,\text{eV}) = 5.25\,\text{eV}. \tag{9}$$

Similarly, the ionization energy (IE) can be calculated by substituting $E_{valence}$ for E_{Fermi},

$$IE = h\nu - (E_{cutoff} - E_{valence}). \quad (10)$$

There are a few ways to determine edges such as E_{cutoff}. A commonly used method is to find the intercept of two lines: one that is fit to the background on the high binding energy side, and a second line fit to the more vertical portion of the cutoff. This approach is not as accurate as calculating the first derivative of the curve to determine E_{cutoff}. UPS data have been particularly useful in the construction of energy diagrams, particularly, for organic electronic devices such as light emitting diodes and photovoltaic cells.[134–136]

IX. SUMMARY: ADVANTAGES AND DISADVANTAGES

XPS is one of the most prominent and widely available surface analysis techniques and applications of this method continue to expand. The two main advantages of the technique are its surface sensitivity (~10nm) and its ability to distinguish differences in chemical environment, characteristics that have uniquely positioned XPS to answer many research questions. XPS can detect all elements except hydrogen and helium with detection limits of approximately 0.1%–1%, is quantitative without standards and is relatively nondestructive. The lateral resolution of a few micrometers to hundreds of micrometers can be informative but is not as good as other techniques such as Auger electron spectroscopy or energy dispersive spectroscopy (EDS) on a scanning electron microscope. Since XPS is extremely surface sensitive, care must be taken to avoid surface contamination. Charging of insulating samples can cause problems, but charge neutralizers help remedy the problem.

While XPS continues to be a very popular tool for surface analysis, care and caution need to be used in interpreting the data. This paper is intended to help clarify many aspects of XPS analysis. However, the cautions noted throughout the paper indicate some of the areas for which greater knowledge can be important. Consultation with knowledgeable XPS analysts and consideration of topics addressed in other guides in this series are recommended to avoid misinterpretation of the data or misrepresentation of the results. As noted throughout the paper, it is important to provide a full description of the instrument, sample, data collection, and analysis methods to enable others to trust and reproduce the results.

ACKNOWLEDGMENTS

This work was performed in part at the Analytical Instrumentation Facility (AIF) and the Chapel Hill Analytical and Nanofabrication Laboratory (CHANL), both of which are supported by the State of North Carolina and the National Science Foundation (Award No. ECCS-1542015). The AIF and CHANL are members of the North Carolina Research Triangle Nanotechnology Network (RTNN), a site in the National Nanotechnology Coordinated Infrastructure (NNCI).

REFERENCES

[1]See: https://avs.scitation.org/toc/jva/collection/10.1116/jva.2020.REPROD2020.issue-1.
[2]D. R. Baer *et al.*, J. Vac. Sci. Technol. A **37**, 031401 (2019).
[3]M. R. Linford *et al.*, Microsc. Microanal. **26**, 1 (2020).
[4]J. F. Watts and J. Wolstenholme, *An Introduction to Surface Analysis by XPS and AES* (Wiley, Chichester, 2020).
[5]D. Briggs, in *XPS: Basic Principles, Spectral Features and Qualitative Analysis in Surface Analysis by Auger and X-ray Photoelectron Spectroscopy*, edited by D. Briggs and J. T. Grant (Surface Spectra, Chichester, 2003), pp. 31–56.
[6]J. F. Watts and J. Wolstenholme, *An Introduction to Surface Analysis by XPS and AES* (Wiley, Chichester, 2003).
[7]D. P. Woodruff and T. A. Delchar, *Modern Techniques of Surface Science*, 2nd ed. (Cambridge University, Cambridge, 1994).
[8]B. D. Ratner and D. G. Castner, in *Electron Spectroscopy for Chemical Analysis in Surface Analysis: The Principal Techniques*, edited by J. C. Vickerman (Wiley, Chichester, 2009), pp. 47–112.
[9]*Practical Surface Analysis*, edited by D. Briggs and M. P. Seah (Wiley, Chichester, 1990), Vol. I.
[10]*Practical Surface Analysis*, edited by D. Briggs and M. P. Seah (Wiley, Chichester, 1983).
[11]W. M. Riggs and M. J. Parker, "Surface analysis by x-ray photoelectron spectroscopy," in *Methods of Surface Analysis*, edited by A. W. Czanderna (Elsevier Scientific Publishing Company, Amsterdam, 1975), pp. 103–158.
[12]A. G. Shard, J. Vac. Sci. Technol. A **38**, 041201 (2020).
[13]C. R. Brundle and B. V. Crist, J. Vac. Sc. Technol. A **38**, 041001 (2020).
[14]C. J. Powell, J. Vac. Sci. Technol. A **38**, 023209 (2020).
[15]M. H. Engelhard, D. R. Baer, A. Herrera-Gomez, and P. M. A. Sherwood "Introductory guide for backgrounds in XPS spectra," J. Vac. Sci. Technol. A (published online).
[16]G. H. Major, N. Farley, P. M. Sherwood, M. R. Linford, J. Terry, V. Fernandez, and K. Artyushkova, "Practical guide for curve fitting in x-Ray photoelectron spectroscopy," J. Vac. Sci. Technol. A (in press).
[17]J. Wolstenholme, J. Vac. Sci. Technol. A **38**, 043206 (2020).
[18]D. R. Baer and A. G. Shard, J. Vac. Sci. Technol. A **38**, 031203 (2020).
[19]R. G. Steinhardt and E. J. Serfass, Anal. Chem. **23**, 1585 (1951).
[20]K. Siegbahn, Phys. Rev. **105**, 1676 (1957).
[21]K. Larsson, E. Sokolowski, and K. Siegbahn, Ark. Fys. **13**, 483 (1958).
[22]K. Siegbahn *et al.*, Nova Acta Reg. Soc. Sci. Upsaliensis **20**, 1 (1967).
[23]B. D. Ratner and D. G. Castner, "Electron spectroscopy for chemical analysis," in *Surface Analysis: The Principal Techniques*, edited by J. C. Vickerman (Wiley, Chichester, 2009), p. 56.
[24]C. D. Wagner, W. M. Riggs, L. E. Davis, J. F. Moulder, and G. E. Muilenberg, *Handbook of X-ray Photoelectron Spectroscopy* (Perkin-Elmer Corporation, Eden Prairie, MN, 1979).
[25]J. F. Moulder, W. F. Stickle, P. E. Sobol, and K. D. Bomben, *Handbook of X-ray Photoelectron Spectroscopy* (Physical Electronics, Inc., Eden Prairie, 1992).
[26]N. Ideo, Y. Iijima, N. Niimura, M. Sigematsu, T. Tazawa, S. Matsumoto, K. Kojima, and Y. Nagasawa, *Handbook of X-ray Photoelectron Spectroscopy* (JEOL, Tokyo, 1991).
[27]G. Beamson and D. Briggs, *High Resolution XPS of Organic Polymers—The Scienta ESCA 300 Database* (Wiley, Chichester, 1992).
[28]The XPS of Polymers Database, edited by G. Beamson and D. Briggs, SurfaceSpectra, United Kingdom, CD-ROM ISBN 0-9537848-4-3
[29]B. V. Crist, *Handbooks of Monochromatic XPS Spectra, 5 Volume Series* (XPS International, Kawasaki, 1997).
[30]B. V. Crist, *Handbook of Monochromatic XPS Spectra: The Elements and Native Oxides* (Wiley, Chichester, 2000).
[31]B. V. Crist, *Handbook of Monochromatic XPS Spectra: Polymers and Polymers Damaged by X-Rays* (Wiley, Chichester, 2000).
[32]B. V. Crist, *Handbook of Monochromatic XPS Spectra: Semiconductors* (Wiley, Chichester, 2000).

[33]Surface Science Spectra (SSS), Spectral data for XPS, AES, and SIMS. An official journal of the American Vacuum Society (AVS), see: https://avs.scitation.org/journal/sss.
[34]X. Llovet, F. Salvat, D. Bote, F. Salvat-Pujol, A. Jablonski, and C. J. Powell, *NIST Database of Cross Sections for Inner-Shell Ionization by Electron or Positron Impact, Version 1.0* (National Institute of Standards and Technology, Gaithersburg, MD, 2014).
[35]NIST X-ray Photoelectron Spectroscopy Database, NIST Standard Reference Database Number 20, National Institute of Standards and Technology, Gaithersburg MD, 20899 (2000), see: https://srdata.nist.gov/xps/main_search_menu.aspx.
[36]XPS Simplified. Thermo Scientific XPS website at www.xpssimplified.com.
[37]XPSSurfA Online collaborative surface analysis database, see: https://cmsshub.latrobe.edu.au/xpsdatabase/spectra/view_many.
[38]M. P. Seah and G. C. Smith, Surf. Interface Anal. **15**, 751 (1990).
[39]P. J. Cumpson and M. P. Seah, Surf. Interface Anal. **25**, 430 (1997).
[40]C. J. Powell, J. Elect. Spectrosc. Rel. Phenom. **47**, 197 (1988).
[41]M. P. Seah and W. A. Dench, Surf. Interface Anal. **1**, 2 (1979).
[42]C. D. Wagner, L. E. Davis, and W. M. Riggs, Surf. Interface Anal. **2**, 53 (1980).
[43]S. Tanuma, "Electron attenuation lengths," in *Surface Analysis by Auger and X-ray Photoelectron Spectroscopy*, edited by D. Briggs and J. T. Grant (Surface Spectra, Chichester, 2003), pp. 259–294.
[44]S. Tanuma, C. J. Powell, and D. R. Penn, Surf. Interface Anal. **17**, 911 (1991).
[45]P. J. Cumpson and M. P. Seah, Surf. Interface Anal. **25**, 430 (1997).
[46]A. Jablonski and C. J. Powell, Surf. Sci. Rep. **47**, 33 (2002).
[47]NIST Standard Reference Database 82, see www.nist.gov/srd/nist-atandard-reference-database-82.
[48]Physical Electronics Quantes Instrument Description, see www.phi.com.
[49]J. F. Watts and J. Wolstenholme, *An Introduction to Surface Analysis by XPS and AES* (Wiley, Chichester, 2020), p. 19.
[50]I. W. Drummond, "XPS: Instrumentation and performance," in *Surface Analysis by Auger and X-ray Photoelectron Spectroscopy*, edited by D. Briggs and J. T. Grant (Surface Spectra, Chichester, 2003), pp. 117–144.
[51]B. D. Ratner and D. G. Castner, "Electron spectroscopy for chemical analysis," in *Surface Analysis: The Principal Techniques*, edited by J. C. Vickerman (Wiley, Chichester, 2009), pp. 80–88.
[52]J. C. Riviere, *Practical Surface Analysis*, edited by D. Briggs and M. P. Seah (Wiley, Chichester, 1990) pp. 19–83, Vol. I.
[53]J. F. Watts and J. Wolstenholme, *An Introduction to Surface Analysis by XPS and AES* (Wiley, Chichester, 2020), p. 47.
[54]J. F. Watts and J. Wolstenholme, *An Introduction to Surface Analysis by XPS and AES* (Wiley, Chichester, 2020), p. 26.
[55]K. Siegbahn, D. Hammond, H. Fellner-Feldegg, and E. F. Barnett, Science **176**, 245 (1972).
[56]D. Briggs, and J. C. Riviere, *Practical Surface Analysis*, edited by D. Briggs and M. P. Seah (Wiley, Chichester, 1990) p. 127, Vol. I.
[57]J. F. Watts and J. Wolstenholme, *An Introduction to Surface Analysis by XPS and AES* (Wiley, Chichester, 2020), pp. 27–30.
[58]D. R. Baer, D. J. Gaspar, M. H. Engelhard, and A. S. Lea, in *Surface Analysis by Auger and X-ray Photoelectron Spectroscopy*, edited by D. Briggs and J. T. Grant (Surface Spectra, Chichester, 2003), pp. 211–233.
[59]M. L. Knotek and P. J. Feibelman, Surf. Sci. **90**, 78 (1979).
[60]D. R. Baer, M. H. Engelhard, and A. S. Lea, Surf. Sci. Spectra **10**, 47 (2003).
[61]Kratos specification for energy resolution on Ag 3d 5/2 is 0.48 eV FWHM.
[62]J. F. Watts and J. Wolstenholme, *An Introduction to Surface Analysis by XPS and AES* (Wiley, Chichester, 2020), p. 52.
[63]B. D. Ratner, P. K. Weathersby, A. S. Hoffman, M. A. Kelly, and L. H. Scharpen, J. Appl. Polym. Sci. **22**, 643 (1978).
[64]A. Takahara, N.-J. Jo, K. Takamori and T. Kajiyama, in *Progress in Biomedical Polymers*, edited by C. G. Gebelein and R. L. Dunn (Plenum, New York, 1990), pp. 217–228.
[65]A. Shchukarev, J. F. Boily, and A. R. Felmy, J. Phys. Chem. C **111**, 18307 (2007).
[66]C. D. Easton, C. Kinnear, S. L. McArthur, and T. R. Gengenbach, J. Vac. Sci. Technol. A **38**, 023207 (2020).
[67]Donald. R. Baer, J. Vac. Sci. Technol., A **38**, 031201 (2020).
[68]J. Geller, in *Surface Analysis by Auger and X-ray Photoelectron Spectroscopy*, edited by D. Briggs and J. T. Grant (Surface Spectra, Chichester, 2003), pp. 89–116.
[69]F. A. Stevie. R. Garcia, J. Shallenberger, J. G. Newman, and C. L. Donley, J. Vac. Sci. Technol. A **38**, 063202 (2020).
[70]K. Siegbahn, Rev. Mod. Phys. **54**, 709 (1982).
[71]J. F. Watts and J. Wolstenholme, *An Introduction to Surface Analysis by XPS and AES* (Wiley, Chichester, 2020), p. 146.
[72]*ASTM E1829-14 Standard Guide for Handling Specimens Prior to Surface Analysis* (ASTM, West Conshohocken, PA, 2014).
[73]*ASTM E1028-02 Standard Guide for Specimen Preparation and Mounting in Surface Analysis* (ASTM, West Conshohocken, PA, 2002).
[74]ISO Standard 18117, *Surface Chemical Analysis—Handling of Specimens Prior to Analysis* (ISO, Geneva, 2009).
[75]ISO 18116, *Surface Chemical Analysis—Guide to Preparation and Mounting of Specimens for Analysis* (ISO, Geneva, 2004).
[76]ISO 20579-4 Surface Chemical Analysis-Guidelines to sample handling, preparation and mounting – Part 4: Reporting information related to the history, preparation, handling and mounting of nano-objects prior to surface analysis (ISO, Geneva 2018).
[77]D. R. Baer, D. J. H. Cant, D. G. Castner, G. Ceccone, M. H. Engelhard, A. S. Karakoti, and A. Muller, in *Characterization of Nanoparticles: Measurement Processes for Nanoparticles*, edited by V.-D. Hodoroaba, W. E. S. Unger, and A. G. Shard (Elsevier, Amsterdam, 2020), p. 316.
[78]J. D. P. Counsell, A. J. Robert, W. Boxford, C. Moffitt, and K. Takahashi, J. Surf. Anal. **20**, 211 (2014).
[79]W. P. Dianis and J. E. Lester, Anal Chem. **45**, 1416 (1973).
[80]C. E. Bryson III, Surf. Sci. **189/190**, 50 (1987).
[81]J. B. Metson, Surf. Interface Anal. **27**, 1069 (1999).
[82]D. R. Baer, M. H. Engelhard, D. J. Gaspar, A. S. Lea, and C. F. Windisch, Jr., Surf. Interface Anal. **33**, 781 (2002).
[83]G. Vereecke and P. G. Rouxhet, Surf. Interface Anal. **26**, 490 (1998).
[84]D. R. Baer *et al.*, J. Vac. Sci. Technol. A **38**, 031204 (2020).
[85]A. J. Pertsin and Y. M. Pashunin, Appl. Surf. Sci. **44**, 171 (1990).
[86]S. Suzer, Anal. Chem. **75**, 7026 (2003).
[87]G. Greczynski and L. Hultman, Prog. Mater. Sci. **107**, 100591 (2020).
[88]D. Shah, D. I. Patel, T. Roychowdhury, G. B. Raynor, N. O'Toole, D. R. Baer, and M. R. Linford, J. Vac. Sci. Technol. B **36**, 062902 (2018).
[89]D. A. Shirley, "Many-electron and final-state effects: Beyond the one-electron picture," in *Photoemission in Solids. I. General Principles*, edited by M. Cardona and L. Ley (Springer-Verlag, Berlin, 1978), pp. 165–195.
[90]J. F. Watts and J. Wolstenholme, *An Introduction to Surface Analysis by XPS and AES* (Wiley, Chichester, 2020), pp. 86–88.
[91]D. Briggs and J. C. Riviere, *Practical Surface Analysis*, edited by D. Briggs and M. P. Seah (Wiley, Chichester, 1990), pp. 127–133, Vol. I.
[92]*ASTM E2108-16 Standard Practice for Calibration of the Electron Binding-Energy Scale of an X-Ray Photoelectron Spectrometer* (ASTM, West Conshohocken, PA, 2016).
[93]*ISO Standard 15472 Surface Chemical Analysis—X-ray Photoelectron Spectrometers—Calibration of Energy Scales* (ISO, Geneva, 2010).
[94]D. A. Shirley, Phys. Rev. B **5**, 4709 (1972).
[95]M. P. Seah, Surf. Sci. **420**, 2 (1999).
[96]*ISO/TR 18392 X-ray Photoelectron Spectroscopy—Procedures for Determining Backgrounds* (ISO, Geneva, 2005).
[97]P. M. A. Sherwood, Surf. Interface Anal. **51**, 589 (2019).
[98]C. D. Wagner, Anal. Chem. **44**, 1050 (1972).
[99]J. H. Scofield, J. Electron Spectrosc. Rel. Phenom. **8**, 129 (1976).
[100]G. C. Smith and M. P. Seah, Surf. Interface Anal. **16**, 144 (1990).
[101]C. D. Wagner, L. E. Davis, M. V. Zeller, J. A. Taylor, R. H. Raymond, and L. H. Gale, Surf. Interface Anal. **3**, 211 (1981).

[102]CasaXPS Manual, 2.3.15 Introduction to XPS and AES, Neal Fairley, Casa Software Ltd. 2009.
[103]A. Shard, Surf. Interface Anal. **46**, 175 (2014).
[104]B. D. Ratner and D. G. Castner, "Electron spectroscopy for chemical analysis," in *Surface Analysis: The Principal Techniques*, edited by J. C. Vickerman (Wiley, Chichester, 2009), p. 50.
[105]W. E. S. Unger, J. Vac. Sci. Technol. A **38**, 021201 (2020).
[106]W. A. Fraser, J. V. Florio, W. N. DeGlass, and W. D. Robertson, Rev. Sci. Instrum. **44**, 1490 (1973).
[107]K. E. Smith and S. D. Kevan, Prog. Solid State Chem. **21**, 19 (1991).
[108]A. I. Martin-Concepcion, F. Yubero, J. P. Espinos and S. Tougaard, Surf. Interface Anal. **36**, 788 (2004).
[109]W. Smekal, W. S. M. Werner, and C. J. Powell, Surf. Interface Anal. **37**, 1059 (2005).
[110]See: https://www.nist.gov/srd/nist-standard-reference-database-100.
[111]S. Tougaard, J. Elec. Spec. Rel. Phenom. **178–179**, 128 (2010).
[112]M. Mohai, Surf. Interface Anal. **36**, 828 (2004).
[113]R. G. Wilson, F. A. Stevie, and C. W. Magee, *Secondary Ion Mass Spectrometry: A Practical Handbook for Depth Profiling and Bulk Impurity Analysis* (Wiley, New York, 1989).
[114]F. A. Stevie, *Secondary Ion Mass Spectrometry: Applications for Depth Profiling and Surface Characterization* (Momentum, New York, 2016).
[115]J. L. Sullivan, S. O. Saied, and I. Bertoti, Vacuum **42**, 1203 (1991).
[116]D. R. Baer *et al.*, J. Vac. Sci. Technol. A **28**, 1060 (2010).
[117]A. G. Shard, F. M. Green, P. J. Brewer, M. P. Seah, and I. S. Gilmore, J. Phys. Chem. B **112**, 2596 (2008).
[118]N. Sanada, A. Yamamoto, R. Oiwa, and Y. Ohashi, Surf. Interface Anal. **36**, 280 (2004).
[119]I. Yamada, J. Matsuo, N. Toyoda, and A. Kirkpatrick, Mater. Sci. Eng. **R34**, 231 (2001).
[120]T. Miyayama, N. Sanada, S. R. Bryan, J. S. Hammond, and M. Suzuki, Surf. Interface Anal. **42**, 1453 (2010).
[121]M. P. Seah and G. C. Smith, Surf. Interface Anal. **11**, 69 (1988).
[122]D. Baer and M. H. Engelhard, Surf. Interface Anal. **29**, 766 (2000).
[123]J. F. Watts and J. Wolstenholme, *An Introduction to Surface Analysis by XPS and AES* (Wiley, Chichester, 2020), p. 61.
[124]L. Zhong, D. Chen, and S. Zafeiratos, Catal. Sci. Technol. **9**, 3851 (2019).
[125]R. M. Palomino, R. Hamyln, Z. Liu, D. C. Grinter, I. Waluyo, J. A. Rodriquez, and S. D. Senanayake, J. Electron Spectros. Rel. Phenom. **221**, 28 (2017).
[126]A. Yulaev, H. Guo, E. Strelcov, L. Chen, I. Vlassiouk, and A. Kolmakov, ACS Appl. Mater. Interfaces **9**, 26492 (2017).
[127]R. Endo, D. Watanabe, M. Shimomura, and T. Masuda, Appl. Phys. Lett. **114**, 173702 (2019).
[128]T. Masuda, Top. Catal. **61**, 2103 (2018).
[129]A. Kolmakov, D. A. Dikin, L. J. Cote, J. Huang, M. K. Abyaneh, M. Amati, L. Gregoratti, S. Gunther, and M. Kiskinova, Nat. Technol. **6**, 651 (2011).
[130]J. Kraus, R. Reichelt, S. Gunther, L. Gregoratti, M. Amati, M. Kiskinova, A. Yulaev, I. Vlassiouk, and A. Kolmakov, Nanoscale **6**, 14394 (2014).
[131]J.-Q. Zhong, M. Wang, W. H. Hoffmann, M. A. van Spronsen, D. Lu, and J. Anibal, Appl. Phys. Lett. **112**, 091602 (2018).
[132]J. Knudsen, J. N. Andersen, and J. Schnadt, Surf. Sci **646**, 160 (2016).
[133]Y. Takagi, T. Uruga, M. Tada, Y. Iwasawa, and T. Yokoyama, Acc. Chem. Res. **51**, 719 (2018).
[134]P. M. A. Sherwood, in *Surface Analysis by Auger and X-ray Photoelectron Spectroscopy*, edited by D. Briggs, J. T. Grant (Surface Spectra, Chichester, 2003), pp. 531–555.
[135]J. J. Pireaux, J. Riga, R. Caudano, and J. Verbist, ACS Symp. Ser. **162**, 169 (1981).
[136]M. Demeter, M. Neumann, and W. Reichelt, Surf. Sci. **454–456**, 41 (2000).
[137]H. Ishii, K. Sugiyama, E. Ito, and K. Seki, Adv. Mater. **11**, 605 (1999).
[138]W. R. Salaneck, M. Logdlund, M. Fahlman, G. Greczynski, and T. Kugler, Mater. Sci. Eng. **R34**, 121 (2001).
[139]D. Cahen and A. Kahn, Adv. Mater. **15**, 271 (2003).